AN INVESTIGATION OF SCALE EFFECTS ON THE SELF-PROPULSION CHARACTERISTICS OF A SUBMARINE

Savas Sezen*[a], Cihad Delen[b], Ali Dogrul[c], Mehmet Atlar[a]

[a] University of Strathclyde
[b] Istanbul Technical University
[c] Turkish Naval Academy, National Defence University

Abstract

This study's main objective is to investigate the scale effect on the benchmark DARPA Suboff submarine hull form's resistance and self-propulsion characteristics. The study's secondary objective is to explore the feasibility of the 1978 ITTC performance prediction method for submarines' power prediction. In achieving both objectives, the CFD methods are utilised. Hence, the flow around the three different scales of the DARPA submarine forms and its propellers, including a full-scale one, is first solved using the steady RANS method with the k-ω SST turbulence model. Verification studies are conducted to determine the uncertainty level of the numerical computations for each scale. The hull resistance, propeller open water and self-propulsion performances are validated with the available experimental data and other numerical studies in the literature for the widely used benchmark submarine model. In the self-propulsion simulations, the propeller flow is modelled using the discretised propeller geometry with the Moving Reference Frame (MRF) approach. Also, the proportional Integral (PI) controller is adopted to find the self-propulsion point efficiently. The scale effects on the hull resistance and its components, nominal wake fraction and self-propulsion characteristics, are explored at two different velocities. The extrapolated numerical results obtained by the 1978 ITTC procedure show that the scale ratio decrease enables better prediction of the self-propulsion characteristics compared to the full-scale CFD predictions. As well as this, the extrapolated self-propulsion characteristics using the model scale results, which are obtained by the CFD computations, are found to be in good agreement with those of the full-scale CFD results. The study, therefore, suggests that the 1978 ITTC performance prediction method can be used in some confidence to extrapolate the performance results from the model to full-scale for the submerged bodies, similar to the surface ships. This study also presents the full-scale self-propulsion characteristics of the benchmark DARPA Suboff form for the first time in the literature using the CFD tool over a realistic range of submarine forward speeds.

Keywords: *DARPA, E1619, Full-scale, RANS, Scale effect, Self-propulsion.*

1. Introduction

The powering performance prediction of a ship is an important step for the design spiral. In general, this prediction can be achieved by numerical simulations or towing tank tests on a model scale. Then, the model scale results are extrapolated to the full-scale (i.e., actual ship) by employing a suitable extrapolation method (e.g. International Towing Tank Conference (ITTC) recommendations and guidelines [1]). However, the extrapolation from the model scale to full-scale is still challenging due to the different flow properties around the hull and propeller. The theoretical requirement for the dynamic similarity (i.e., Reynolds and Froude similarity) is the well-known challenge between the model and full-scale ships since this cannot be satisfied simultaneously in the towing tank tests. Thus, the associated scale effect phenomenon has been still occupying the naval architecture community [1–3].

Despite the fact that the systematic towing tank experiments and empirical methods are being used to predict the ship powering performance at the early design stages, nowadays, the Computational Fluid Dynamics (CFD) methods have been commonly used as the state-of-art numerical modelling procedures. In this regard, the workshop on CFD in Ship Hydrodynamics [4] has been organised every five years to present the development of CFD tools in model scale and validation of the numerical methods with the experimental data. With increased confidence for the validation of the numerical results in model scale, the numerical simulations have also been commenced to perform in the full-scale to explore the scale effects and avoid them. However, the validation of full-scale numerical results is rare due to the lack of available sea trial data. In order to compare the capabilities of full-scale CFD solutions with the sea trial data, a workshop [5] was organised by Lloyd's Register with the participation of different facilities and universities. Although there are few studies in the literature for the validation of full-scale CFD results with the sea trial data (e.g. Ponkratov et al. [6], Mikkelsen et al. [7]), the full-scale CFD results are generally scarce and compared with those of extrapolated model scale data.

Increasing CFD capabilities for the computation of resistance and self-propulsion characteristics in the model and full scale reveal new research areas to study the model-ship correlations and scale effects. The numerical studies for the investigation of scale effects mainly focused on the bare hull resistance, its components and form factor using viscous solvers in the literature. Terziev et al. [8] examined the scale effect on the resistance components for the benchmark KRISO Container Ship (KCS) using three scales. In this study, the multiphase and double body analyses were performed to examine the resistance and its components. The results showed the ship wave resistance changed considerably with the Reynolds number. Dogrul et al. [9] studied the scale effects on the KCS hull form's resistance components. The extrapolated results were compared with the full-scale numerical results, and the

different decomposition methods were discussed. It was found that the Froude and Hughes extrapolation methods presented different results for the ships which have different block coefficients. In another numerical study, the scale effects on the KCS and Wigley hull forms' resistance components were investigated by Zeng et al. [10], including the shallow water conditions. This study presented a relationship between the wave and frictional resistance and demonstrated that the wave resistance's scale effects could be eliminated with an increase in model length. Delen and Bal [11] focused on the scale effects using Telfer's GEOSIM method for three different KCS models, including the full-scale through the total ship resistance. The authors revised the original Telfer's geosim formulation. The full-scale numerical results were compared with those of the model scales' extrapolated results using both the ITTC extrapolation method and revised Telfer's geosim method. The comparisons showed that the revised method presented better results than the conventional ITTC extrapolation method.

When the hull is incorporated with the propeller to predict the self-propulsion characteristics, the overall velocity and pressure fields near the ship's stern change significantly. From the CFD point of view, one of the challenges is to model the propeller-hull interaction accurately. In the numerical prediction of the ship flow, including a propeller, the propeller's action can be modelled either using an actuator disc concept or fully discretised actual propeller geometry. In the latter approach, the propeller rotational motion can be modelled with one of the well-known modelling techniques: the sliding mesh, MRF, and dynamic overset grid techniques. Although the actuator disc approach is a simplified and computationally affordable technique, inevitably, the modelling of the entire propeller geometry (i.e., latter approach) is more realistic to include the full details of the propeller and hence the real physics of the propeller-hull interaction phenomenon.

The self-propulsion characteristics of the surface ships (e.g. KCS, Duisburg Test Case (DTC) and bulk carriers) have been widely predicted in model scale using different propeller modelling techniques [12–15]. In addition to these studies, the full-scale CFD simulations were performed to predict the self-propulsion characteristics and the investigation of scale effects [1,2,16,17]. Starke et al. [18] employed a RANS/BEM hybrid approach to examine the scale effects on the self-propulsion performance of KCS. The model and full-scale analyses were conducted in their study, and scale effects were found on the nominal wake field, propeller revolution, and forces. The extrapolated results were found to be in good agreement with those of full-scale CFD. Farkas et al. [19] investigated the resistance and self-propulsion characteristics of a bulk carrier. The results of the model experiments were extrapolated to full-scale and then compared with the full-scale CFD data. In their study, different extrapolation methods [20,21] were applied, and the results were discussed in terms of the resistance and self-propulsion point. Lin and Kouh [22] examined the scale effects on the thrust deduction factor. For this

purpose, they conducted self-propulsion analyses for a medium speed containership in different model scales, including the full-scale. The effects of different turbulence models on propeller global performance characteristics, resistance and nominal wake were examined. As a result of this study, the new propulsion analysis procedure was proposed to eliminate the scale effects on the thrust deduction factor. Zhao et al. [23] studied the flow around a ship with two pusher type podded propulsors. The model and full-scale self-propulsion performance were predicted using the numerical tool. The model scale results were extrapolated to full-scale and compared with the full-scale CFD data in a wide range of ship speeds. It was concluded that the 1978 ITTC performance prediction method was suitable for the vessels equipped with the podded propulsors. Delen et al. [24] investigated the ONR Tumblehome geometry's self-propulsion performance using the geosim models. The numerical results showed that Telfer's geosim method showed better accuracy when compared with the 1978 ITTC performance prediction method for predicting the full-scale powering performance of a ship. It was found that the 1978 ITTC performance prediction method more accurately predicted the rotation rate and thrust of a ship in full-scale, whereas the difference in torque characteristics was high.

Apart from the powering performance prediction of surface ships, the prediction of hull-propeller interaction for the submerged bodies (e.g., submarines, AUVs etc.) is also vital for the determination of a suitable and effective method for the powering performance prediction. Within this context, the accurate simulation of the flow field around the submarine is desirable to meet the design requirements for maximum speed, low acoustic signature and stealth mode of operations [25]. Thus, the submarine design is considered a complex and demanding task due to the number of crucial requirements (e.g., low acoustic signature, high propulsion efficiency, and high manoeuvrability). In the literature, numerical studies have been generally conducted using the benchmark DARPA appended and bare hull forms in model scale to predict resistance and self-propulsion characteristics using different numerical tools. In this regard, Chase and Carrica [26,27] examined the DARPA Suboff appended form's self-propulsion performance using the CFDShip-Iowa numerical solver. Also, the authors investigated the effects of grid resolution, the turbulence model on the wake. The results showed that the RANS method was more dissipative than other turbulence models, resulting in unphysically unstable tip vortex formation in the propeller's slipstream. Zhang and Zhang [28] explored the self-propulsion and resistance characteristics of a submarine in the fully submerged and near to the free surface condition. The numerical results were validated with the experimental data. It was concluded that the free surface had more pronounced effects on the resistance than the self-propulsion characteristics. Sezen et al. [29] predicted the total resistance and self-propulsion performance of bare and appended DARPA Suboff forms with E1619 propeller using the RANS method. In the self-propulsion simulations, the actuator disc and discretised propeller were used for

a wide range of forward speeds. The results showed that the self-propulsion characteristics were found slightly high when the actuator disc approach was used compared to the discretised propeller itself. Posa and Balaras [30] solved the flow around the DARPA Suboff submarine form in towed and self-propelled conditions using the LES method. The comparison of the towed and self-propelled conditions was presented. It was found that the boundary layer development over the mid-section of the cylindrical body was nearly unaffected by the propeller suction. However, the impact over the stern was found to be high on the development of the boundary layer. Ozden et al. [31] conducted an experimental study in ITU (Istanbul Technical University) Ata-Nutku Towing tank to predict the appended DARPA Suboff form's self-propulsion characteristics. Also, the numerical calculations were performed using the RANS method. The obtained numerical results were validated with the experimental data at one forward speed in terms of the self-propulsion characteristics. In the study of Carrica et al. [32], Joubert BB2 generic submarine form was chosen for the prediction of self-propulsion performance. The numerical analyses were carried out considering the submarine moving near the free surface in calm water and regular wave conditions. The authors concluded that the hull and free surface interaction caused fluctuations in the wake and propeller thrust. Wang et al. [33] investigated the flow field around DARPA Suboff with E1658 model propeller. The model experiments and numerical analyses were conducted considering the free surface effects in different depths. The Particle Image Velocimetry (PIV) measurements and numerical results showed that the free surface influenced the tip vortex structures significantly in shallow depths, leading to instability of the vortex structures in the propeller's slipstream. Lin and Li [34] solved the turbulent flow field around DARPA Suboff hull form using the unsteady RANS with k-ω turbulence model. In the numerical calculations, the sliding mesh technique was utilised. This study aimed to show the numerical solver's capabilities predicting the hydrodynamic characteristics of this hull form in terms of resistance, vorticity, frictional and pressure coefficients. The results indicated that the friction coefficient decreased with an increase in the Reynolds number. In contrast, the pressure coefficient varied slightly with an increase in the Reynolds number. Zou et al. [35] predicted the self-propulsion performance of an unmanned semi-submerged vessel with a Ka4-70 duct using the RANS method. It was shown that the propulsion efficiency of the ducted propeller was higher than conventional propeller. However, it was stated that the asymmetric velocity distribution at the propeller plane created by the duct triggered the noise and vibration. Paredes et al. [36] investigated the flow around submerged bodies near free surface. The numerical method was first verified and validated for DARPA Suboff submarine form. Later on, the flow around the full-scale Type 209/1300 class submarine form was solved at various depths and Froude numbers. The free surface effects on the total resistance were investigated comprehensively at surface, periscope, and fully submerged depth conditions.

As one can notice, most of the studies reviewed above mainly focused on the surface ships' resistance and self-propulsion characteristics both in the model and full scales. There are also some studies focused on the powering performance predictions of submarines on a model scale. However, the submarine related studies are still limited in model scale. To the best of the authors' knowledge, the full-scale benchmark DARPA Suboff form's self-propulsion characteristics have not been investigated yet. Therefore, one of the present study's novelties is to investigate the self-propulsion performance characteristics of this benchmark submarine form in the full-scale using a CFD approach for a wide range of representative submarine speeds for the first time. Furthermore, it is a well-known fact that, despite its origin for the single screw mono-hull surface ships, the 1978 ITTC powering prediction method has been applied successfully for many twin screws and even for multi-hull surface ships for practical purposes (e.g., NPL Catamarans). However, its applicability for the submerged bodies has not been explored yet. Thus, another novelty of the present study is to examine the feasibility of applying the 1978 ITTC procedure for the powering prediction of a submarine for the first time and associated scale effects.

In order to achieve the above-outlined objectives, in this study, the steady Reynolds-averaged Navier Stokes (RANS) solver was used for the solution of the flow field around the submarine in fully and deeply submerged condition (i.e., there is no wave resistance). The k-ω Shear Stress Transport (SST) turbulence model was selected. Two different model scale submarine forms were generated using the generic DARPA submarine form to investigate the scale effects. The flow around the model and full-scale DARPA Suboff forms propelled by the INSEAN E1619 propellers was first solved. A verification study was performed to determine the numerical calculations' uncertainty level by using the GCI (Grid Convergence Index) method for the resistance simulations in each scale. The total resistance and self-propulsion results obtained with the numerical solver were validated with the available experimental data and other numerical studies in the literature for this widely used scaled model submarine form. Also, the global performance characteristics (i.e., thrust, torque coefficients and efficiency) of the model and full-scale propellers were validated using the model scale open water test data. In the self-propulsion simulations, the PI controller was used for the accurate and efficient determination of the self-propulsion points. The scale effects on the bare hull resistance and its components as well as on the nominal wake and self-propulsion characteristics, were investigated in detail at two different velocities. The self-propulsion characteristics and total resistance values in full-scale were compared with the extrapolated model scale data using the 1978 ITTC procedure at two forward speeds. Consequently, the self-propulsion characteristics of the full-scale DARPA Suboff form was provided for a wide range of representative submarine forward speeds.

The details of the above-outlined investigations are presented in the following six sections of the paper. Section 2 describes the main particulars of the submarine and propeller geometries. The numerical modelling is presented in Section 3. The verification of the CFD solver is given in Section 4. The results and concluding remarks are presented in Section 5, while the conclusions are included in Section 6.

2. Submarine and Propeller Geometry

The well-known benchmark submarine model introduced by the Defense Advanced Research Projects Agency (DARPA) was selected in this study. Also, the experiments were conducted in the towed conditions both in the wind tunnel and towing tank for the DARPA submarine hull forms [37–40]. The appended submarine form is also known as the AFF-8 configuration that includes the sail and rudder fins. The 3D model of the submarine is presented in Figure 1, while its main particulars are given in Table 1 in three different scales. The geometric properties and detailed information of the submarine form can be found in [37]. The benchmark INSEAN E1619 propeller was used for the self-propulsion simulations. The 3D view of the propeller can be seen in Figure 2, whereas the main geometrical properties of the propellers are given in Table 2.

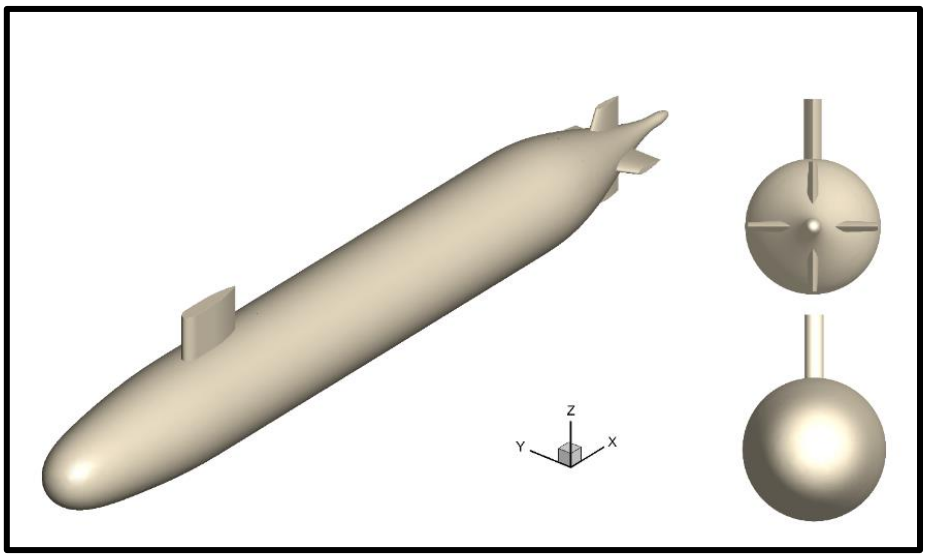

Figure 1*. Representation of DARPA Suboff AFF-8 submarine form.*

Table 1. *Main Particulars of DARPA Suboff AFF-8 forms.*

Main Particular	**Symbol**	**Model1**	**Model2**	**Full**
Scale	λ	24	2	1
Length overall	L_{OA} (m)	4.356	52.272	104.544
Length between perpendiculars	L_{PP} (m)	4.261	51.132	102.264
Maximum diameter	D_{max} (m)	0.508	6.096	12.192
Wetted surface area	S (m^2)	6.348	914.120	3656.480
Displacement	∇(m^3)	0.706	1219.968	9759.744

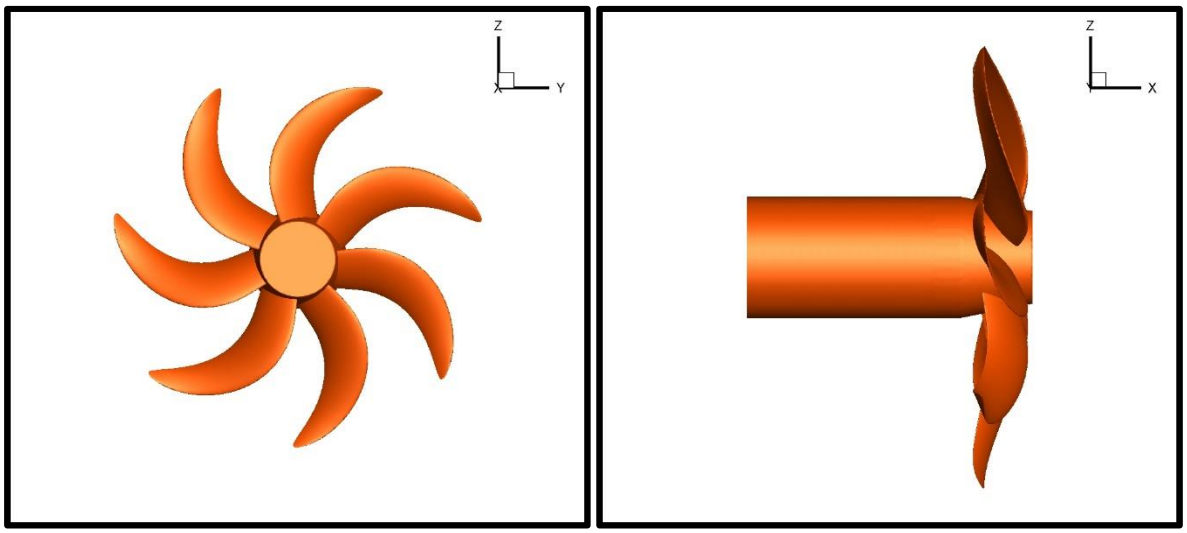

Figure 2. *3D view of INSEAN E1619 propeller.*

Table 2. *Main Particulars of E1619 propellers*

Main Particular	Symbol	Model1	Model2	Full
Scale	λ	24	2	1
Diameter	D (m)	0.262	3.144	6.288
Pitch ratio	P/D		1.15	
Number of blades	Z		7	
Hub diameter ratio	D_h/D		0.226	
Expanded area ratio	A_E/A_0		0.608	
Rotation	-		Right handed	

3. Numerical Modelling

3.1. Governing Equations

The computational fluid dynamics method used for flow modelling is based on the discretisation of the Navier-Stokes equations. Numerical solution of RANS equations and the continuity equation are used to obtain the velocity and pressure fields. The continuity equation is given as follows.

$$\frac{\partial U_i}{\partial x_i} = 0 \tag{1}$$

The mean momentum equation can be written in tensor notation and Cartesian coordinates with the following equation.

$$\frac{\partial U_i}{\partial t} + U_j \frac{\partial U_i}{\partial x_j} = -\frac{1}{\rho}\frac{\partial P}{\partial x_i} + \frac{\partial}{\partial x_j}\left[\upsilon\left(\frac{\partial U_i}{\partial x_j} + \frac{\partial U_j}{\partial x_i}\right)\right] - \frac{\partial \overline{u_i' u_j'}}{\partial x_j} \tag{2}$$

where, ρ depicts the fluid density, kg/m^3; U_i is the velocity, m/s; P represents the pressure, Pa; υ is the kinematic viscosity, m^2/s. The last two terms belong to the viscous stress tensor and Reynolds stress tensor, respectively. Reynolds stress tensor (i.e., $\overline{u_i' u_j'}$) and the kinematic eddy viscosity ($i.e., \upsilon_t$) can be written as follows.

$$\overline{u_i' u_j'} = -\upsilon_t \left(\frac{\partial U_i}{\partial x_j} + \frac{\partial U_j}{\partial x_i} \right) + \frac{2}{3} \delta_{ij} k \tag{3}$$

$$\upsilon_t = \frac{k}{\tilde{\omega}} \tag{4}$$

To simulate the turbulent flow, $k - \omega$ turbulence model [41,42] is used. The transport equations of this model are given below.

$$\frac{\partial k}{\partial t} + U_j \frac{\partial k}{\partial x_j} = \frac{\partial}{\partial x_j} \left[\left(\upsilon + \sigma^* \frac{k}{\omega} \right) \frac{\partial k}{\partial x_j} \right] + P_k - \beta^* k\omega \tag{5}$$

$$\frac{\partial \omega}{\partial t} + U_j \frac{\partial \omega}{\partial x_j} = \frac{\partial}{\partial x_j} \left[\left(\upsilon + \sigma \frac{k}{\omega} \right) \frac{\partial \omega}{\partial x_j} \right] + \alpha \frac{\omega}{k} P_k - \beta \omega^2 + \frac{\sigma_d}{\omega} \frac{\partial k}{\partial x_j} \frac{\partial \omega}{\partial x_j} \tag{6}$$

Here, k depicts the turbulent kinetic energy while ω stands for the dissipation of this energy. P_k is the production rate of turbulent kinetic energy.

$$P_k = -\overline{u_i' u_j'} \frac{\partial U_i}{\partial x_j} \tag{7}$$

The closure coefficients given $(\alpha, \beta, \beta^*, \sigma, \sigma^*, \sigma_d)$in the equations (3-4) and their auxiliary relations can be found in Wilcox [42] in detail.

3.2. Computational Domain and Boundary Conditions

The computational domain was created around the submarine to solve the flow field both in the model and full-scale forms. Numerical analyses were performed using the cartesian coordinate system with the origin located in the aft peak of the submarine form as shown in Figure 3. The domain dimensions were determined following the ITTC recommendation [43]. The upstream and downstream of the domain were extended $2.5L_{PP}$ and $6L_{PP}$ from the aft peak of the form, respectively. In addition, the length of top and bottom sides of the domain were set to $2L_{PP}$ from the centre of the submarine form. For the open water propeller performance simulations, the cylindrical computational domain was used. The upstream of the domain was extended $4D$, whereas the downstream of the domain was set to $11D$. The diameter of the domain was identified as $4D$. Figure 3 shows the computational domain and boundary conditions for the submarine forms (i.e., for the resistance and self-propulsion simulations) and the propellers (i.e., open water simulations). The positive X directions were identified as velocity inlet, whereas the negative X directions were defined as pressure outlet for both computational domains. The remaining surfaces were identified as symmetry planes. The submarine hull and propeller blades were defined as a wall with the no-slip condition to satisfy the kinematic boundary condition.

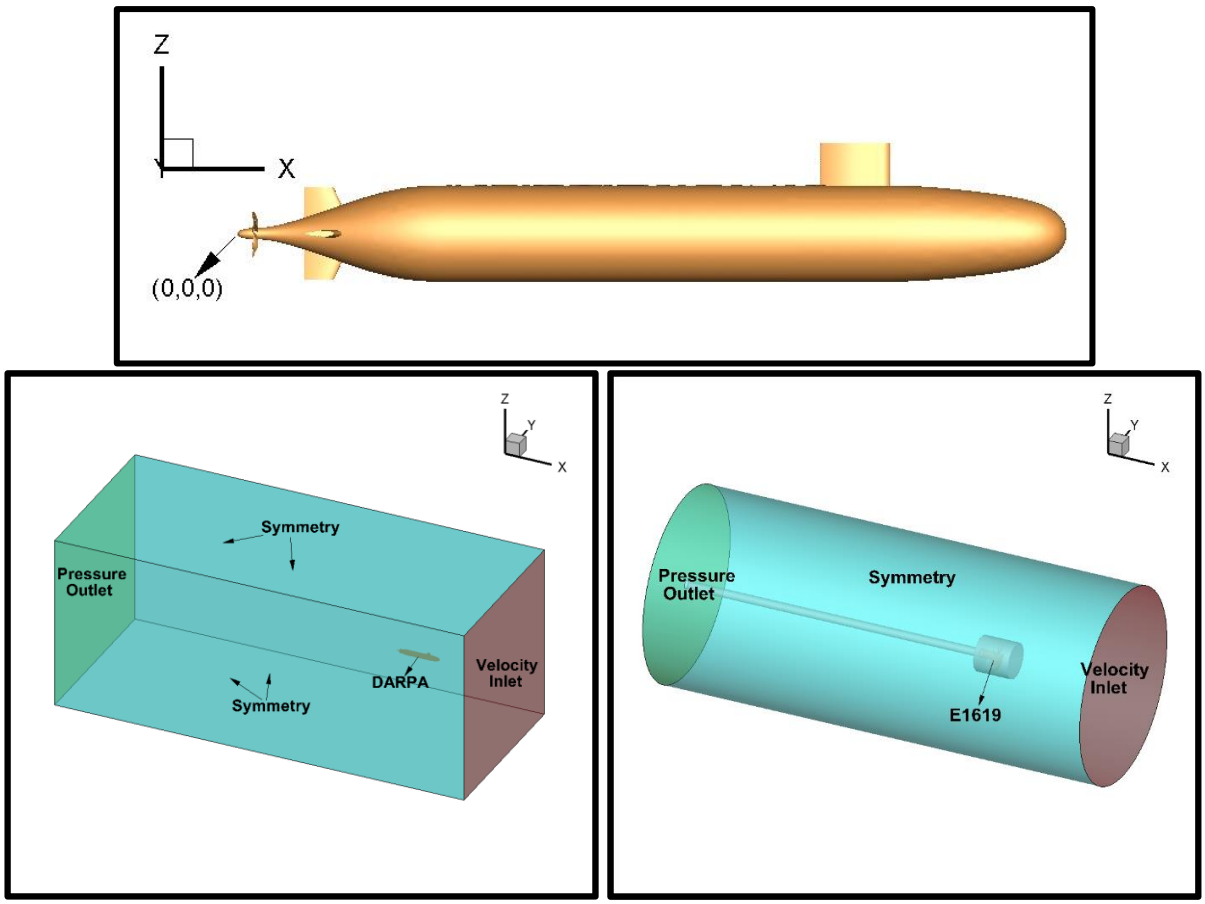

Figure 3. *Self-propulsion geometry with reference frame, Computational domain and boundary conditions (Left: Resistance and Self Propulsion Simulations; Right: Open Water Simulations)*

3.3. Grid Structure

Implementing a suitable grid structure can be considered one of the difficulties in most hydrodynamic modelling problems in CFD. The region-based mesh tool of Star CCM+ [44] was used to discretise the computational domain with the finite volume method. The trimmer mesh with hexahedral elements was adopted in the whole computational domain for the resistance, open water propeller and self-propulsion simulations. The additional mesh refinements in the submarine's wake and around the appendages were adopted to capture the possible flow separations and high-velocity gradients. Additionally, the mesh refinement was also implemented around the propeller blades to solve the flow field precisely. Prism layers were utilised on the solid surfaces along with the submarine forms and propellers for a better representation of the boundary layer. The unstructured grid structure around the submarine forms and propellers is given with the close-up views in the aft and bow proximity, as shown in Figure 4 and 5. The total mesh (element) numbers used in the self-propulsion simulations are 2.1M, 2.3M and 2.7M for Model 1 (i.e., λ=24), Model 2 (i.e., λ=2), and full-scale (i.e., λ=1), respectively. The same grid structures of the open water propeller and resistance simulations were used for the self-propulsion simulations.

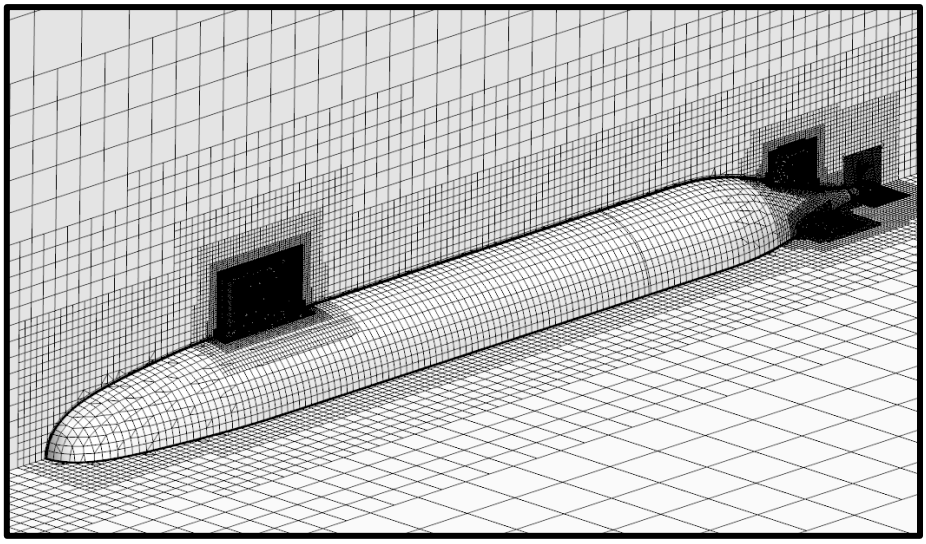

Figure 4. *Grid structure around the submarine.*

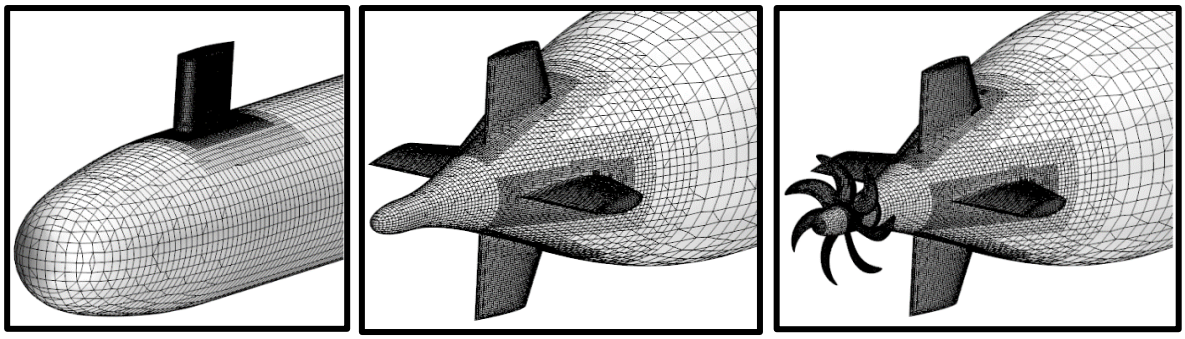

Figure 5. *Close-up views of grid structure on the bow and stern of the submarine.*

3.4. Solution Methodology

The commercial CFD software package, Star CCM+, was utilised in numerical computations. The governing equations were discretised using the finite volume method. A second-order scheme is applied for spatial discretisation. The SIMPLE algorithm was used for velocity-pressure coupling. The k-ω SST turbulence model with all wall y^+ treatment method was used to model the turbulent flow field. The k-ω SST turbulence model makes use of the pros of standard k-ω and k-ε turbulence models. The k-ω formulation is used in the inner parts of the boundary layer. In contrast, the k-ε behaviour is provided for the accurate solution of the near-wall with the low sensitivity of the turbulence properties. Consequently, these advantages bring an accurate prediction for the solution of adverse gradients and separating flows [45]. Detailed information about the turbulence model can be found in the commercial solver's user guide [44]. The prism layer numbers used in the simulations for the submarine hull forms were changed between 5 and 10 with a growth ratio of 1.5, yielding an average y^+ value between 65 and 600 depending on the scale and velocity. Additionally, the prism layer numbers were selected between 4 and 8 for the propellers with a growth ratio of 1.5. Thus, the average y^+ values vary between 40 and 300 for three different propeller scales in open water

conditions. The wall y^+ distribution on the full-scale hull form is given at maximum forward speed investigated in this study in Figure 6.

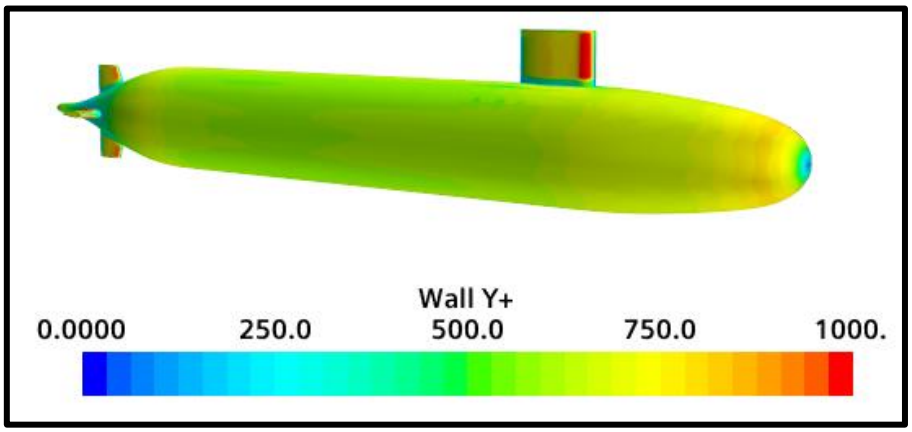

Figure 6. *The wall y^+ distribution on the full-scale submarine form at 29knots.*

In this study, the MRF approach was used to model the propeller rotational motion used in many CFD problems with rotating regions. The MRF approach provides steady approximation, and it is considered less computationally expensive compared to the sliding mesh technique. In this approach, the MRF zone is rotated around the body while the body is kept constant. As stated in the literature (e.g., [46,47]), the MRF approach is preferred instead of the sliding mesh and overset mesh techniques if the flow's unsteady behaviours are not of great interest. In this study, as the free surface effects were ignored and the submarine was assumed fully submerged, the self-propulsion simulations were conducted using the MRF approach in a steady manner to reduce the computational cost of the simulations. The flow chart of the numerical steps implemented in this study is shown in Figure 7.

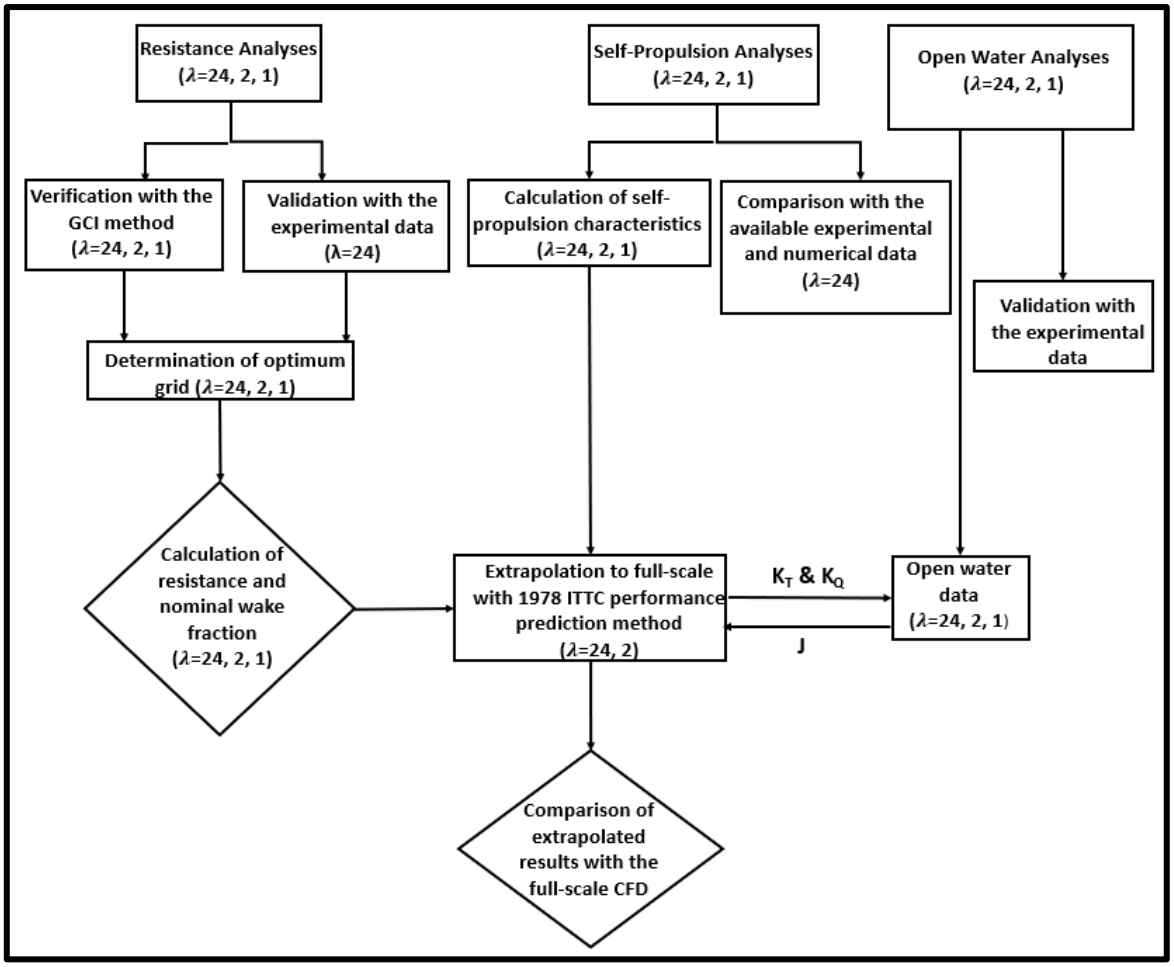

Figure 7. *The flow chart for the numerical simulations.*

3.5. PI (Proportional-Integral) Controller

In a typical self-propulsion test, the model is towed for a given target speed, and propeller speed is adjusted to zero the net force acting along the propeller shaft under the effect of the ship resistance and propeller's thrust, and hence specifying the self-propulsion point [48,49]. Having achieved the balance between the resistance and propeller's thrust, the self-propulsion characteristics can be evaluated at this balance (i.e., self-propulsion) condition in model scale and then extrapolated to the full-scale using appropriate procedures. One of the disadvantages of this approach in the simulations using a CFD solver is that it requires several runs at varying propeller rotational speeds for the given ship speed to obtain the self-propulsion point. As this approach increases the computational cost, a PI controller can be a cost-effective alternative to control the propeller speed and rapidly to find the self-propulsion point described as follows.

The general formulation of the controller can be expressed as follows.

$$n(t) = n_0\left(1 + K_p \cdot error + K_i \sum error\right) \tag{8}$$

Here, n_0 is the initial value of the propeller rotational speed, rps; t is the time, s. K_i and K_p are the gains for the integral and proportional parts of the PI controller, respectively. The error is the difference between the target output and the current output value. In our case, the error can be the difference between the total resistance (R_T) and propeller thrust (T) with the following formulation.

$$e = R_T - T \tag{9}$$

It should be noted that the selection of the K_i and K_p values have an impact on the stability and convergence rate of the PI controller. To increase the convergence speed of the simulation (i.e., decrease the computational cost), the optimal values of the K_i and K_p values can be found easily with trial and errors. In this study, the K_i and K_p values were set to 10^{-8} for Model 2 and full-scale, whereas 10^{-5} was chosen for Model 1.

4. Verification of the CFD Approach

A verification study was conducted to assess the uncertainty of the numerical results at different scales using the Grid Convergence Index (GCI) technique, which is based on the Richardson extrapolation method [50]. In this technique, the numerical solution is predicted with zero grid spacing by using the solutions of systematically refined grids; thus, it calculates the solution's numerical error. The method was first proposed by Roache [51], and it has been commonly implemented by using the procedure given by Celik et al. [52] in the literature. This technique was also recommended by ITTC [53,54] and AIAA [55] for uncertainty assessment of the numerical calculations and it has been used in several studies (e.g., [29,56]).

Numerical solutions were obtained using three different sets of grid resolution to determine the uncertainty level of the numerical calculation. The grid resolution is refined and coarsened in all directions. In this technique, the refinement factor (r) was selected as $2^{0.5}$, which is generally employed in CFD applications. Besides, it is recommended to use a refinement factor greater than 1.3. The difference between the solution scalars (ε) can be found using the following Equation,

$$\varepsilon_{21} = \varphi_2 - \varphi_1, \quad \varepsilon_{32} = \varphi_3 - \varphi_2 \tag{10}$$

Here, φ_1, φ_2, φ_3 indicate the numerical results for the fine, medium, and coarse grid solution, respectively. The solution scalar was selected as a non-dimensional total resistance coefficient both in the model scales (i.e., Model 1 and Model 2) and full-scale in bare hull condition at V_{M1}=3.051 m/s (λ=24), V_{M2}=10.57 m/s (λ=2), and V_S=14.95 m/s (λ=1). In the uncertainty study, the near-wall properties (i.e., prism layer mesh) around the hull were kept constant, and the grid density was changed systematically with the refinement factor of $2^{0.5}$ as recommended for the GCI method.

Convergence conditions of the numerical solution can be calculated as follows,

$$R = \frac{\varepsilon_{21}}{\varepsilon_{32}} \tag{11}$$

The determination of the solution can be assessed according to the range of R values [57]. Oscillatory convergence: -1 < R < 0, monotonic convergence: 0 < R < 1, oscillatory divergence: R < -1 and monotonic divergence: R > 1.

The extrapolated value can be calculated using the following Equation 12.

$$\varphi_{ext}{}^{21} = (r^p \varphi_1 - \varphi_2)/(r^p - 1) \tag{12}$$

where p is the apparent order of accuracy and calculated using the following Equation 13.

$$p = \frac{1}{In(r_{21})} |In|\varepsilon_{32}/\varepsilon_{21}| + q(p)| \tag{13}$$

Here, $q(p)$ and s can be defined as follows.

$$q(p) = In(\frac{r_{21}{}^p - s}{r_{32}{}^p - s}) \tag{14}$$

$$s = sgn(\varepsilon_{32}/\varepsilon_{21}) \tag{15}$$

The approximate and extrapolated relative errors are also defined as follows,

$$e_a{}^{21} = \left|\frac{\varphi_1 - \varphi_2}{\varphi_1}\right| \quad e_{ext}{}^{21} = \frac{|\varphi_{ext}{}^{12} - \varphi_1|}{\varphi_{ext}{}^{12}} \tag{16}$$

Finally, the uncertainty level of the numerical solution can be calculated by,

$$GCI_{fine}{}^{21} = \frac{1.25 e_a{}^{21}}{r_{21}{}^p - 1} \tag{17}$$

The element counts and solution of the scalars for each grid structures and the numerical study's uncertainty level for both model and full-scale submarine forms are given in Table 3.

Table 3. *Verification study of different submarine forms in terms of total resistance.*

Parameter	C_T (λ=24)	C_T (λ=2)	C_T (λ=1)
N_1	982300	1100030	1270488
N_2	564431	642985	767315
N_3	367968	411395	474216
r_{12}	1.202	1.196	1.183
r_{32}	1.153	1.160	1.174
φ_1	3.355E-3	2.207E-3	1.970E-3
φ_2	3.422E-3	2.239E-3	1.996E-3
φ_3	3.542E-3	2.326E-3	2.087E-3
q	0.280	0.199	0.051
p	3.945	5.984	7.422
R	0.557	0.368	0.291
${\varphi_{ext}}^{21}$	3.292E-3	2.190E-3	1.960E-3
${e_a}^{21}$	2.002E-2	1.449E-2	1.331E-2
${e_{ext}}^{21}$	1.902E-2	7.615E-3	5.395E-3
GCI_{FINE} (%)	2.334	0.945	0.671

According to the results shown in Table 3, the highest uncertainty was computed approximately 2% at Model 1. As a result of the uncertainty study, the fine grid structures were selected for the resistance and self-propulsion simulations for the model and full-scales.

5. Results and Discussion

5.1. Open water propeller analysis

The open water performance of E1619 propeller in different scales was predicted at three different advance ratios (i.e., J=0.8505, J =0.8909 and J =0.9661) as these three advance ratios cover the self-propulsion range for the thrust identity method. The advance ratio (J), non-dimensional thrust (K_T) and torque coefficients ($10K_Q$) and efficiency values were calculated using the following equations.

$$J = \frac{V_A}{nD} \tag{18}$$

$$K_T = \frac{T}{\rho n^2 D^4} \tag{19}$$

$$K_Q = \frac{Q}{\rho n^2 D^5} \tag{20}$$

$$\eta_0 = \frac{J}{2\pi}\frac{K_T}{K_Q} \tag{21}$$

Here, V_A is the averaged flow (or advance) velocity at the propeller plane, m/s; n is the propeller rotational speed, rps; Q is the torque, Nm. Figure 8 compares the numerical predictions with the

experimental data for the thrust and torque coefficients and the propeller efficiency for each scale ratio. It should be noted that the experimental values for the INSEAN E1619A model propeller were measured at D=0.485m ($\lambda = 13$) in open water conditions. The deviations between the CFD and experimental values were found around 1-7% for different scales for the thrust and torque coefficients. The propeller rotational speeds were set to 1.388rps, 1.963rps and 6.802rps for the full-scale propeller, Model 2, and Model 1, respectively, using the experimental propeller rotational speed for the D=0.485m ($\lambda = 13$) with the help of Froude similarity. The incoming velocity was changed according to the advance ratio (i.e., J).

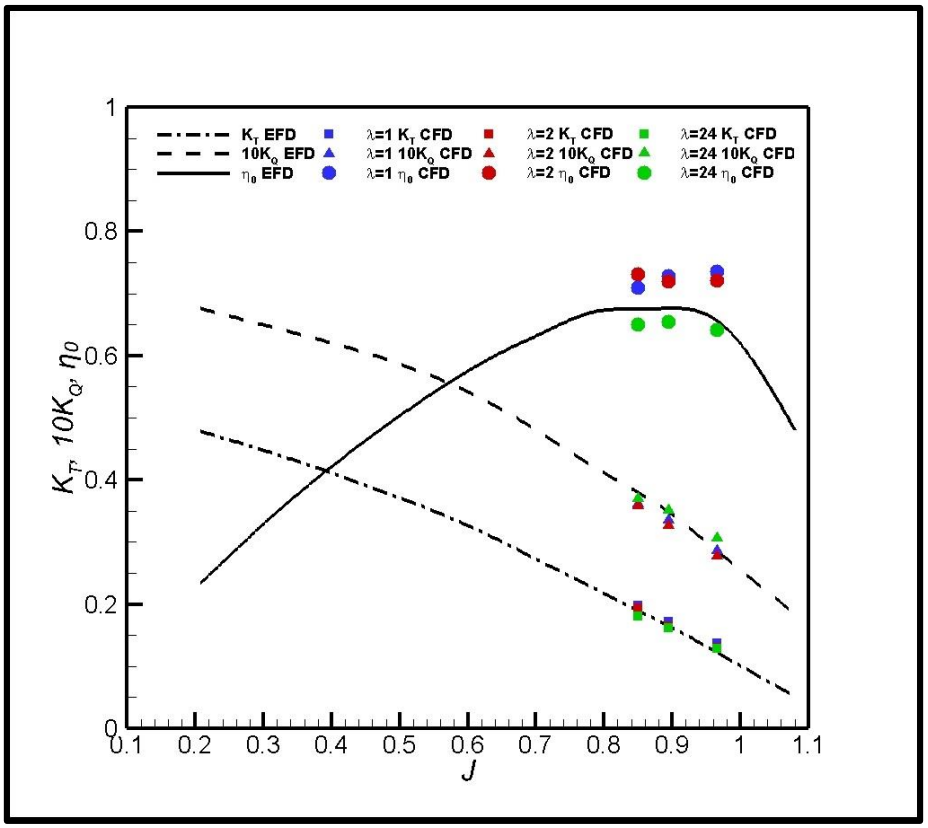

Figure 8. *Comparison of global performance characteristics with the EFD (Experimental Fluid Dynamics) for different scales.*

5.2. Resistance analysis

According to the Froude assumption, the total resistance of the vessel (R_T) can be written as the summation of the frictional resistance (R_F) and residual resistance (R_R):

$$R_T = R_F + R_R \tag{22}$$

The residual resistance (R_R) includes the viscous pressure resistance (R_{VP}) which occurs due to the separation and energy losses created by the eddy motion and the wave resistance (R_W):

$$R_R = R_{VP} + R_W \tag{23}$$

On the other hand, according to Hughes' assumption (i.e., forms basis for the 1978 ITTC procedure), the vessel's total resistance comprises three components: frictional resistance, viscous pressure resistance, and wave resistance, as defined in Equation 24. Here, $(1 + k)$ denotes the form factor at each velocity and scale.

$$R_T = R_F + R_{VP} + R_W = (1 + k)R_F + R_W \tag{24}$$

As the submarine is assumed fully submerged, the wave resistance component (R_W) was ignored in this study. The total resistance and its components can be written in a non-dimensional form by dividing each term to the dynamic pressure and wetted surface area. The residuary resistance component can be considered as a function of the Froude number (Fr), whereas the frictional resistance component is a function of Reynolds number (Re). Hence, the non-dimensional form of Equation 22 can be written as:

$$C_T = C_F(Re) + C_R(Fr) \tag{25}$$

Where the frictional resistance coefficient can be predicted using the 1957 ITTC correlation line [20]:

$$C_F = \frac{0.075}{[\log(Re) - 2]^2} \tag{26}$$

The Reynolds (Re) and Froude (Fr) numbers are defined as follows;

$$Re = \frac{VL}{\upsilon} \tag{27}$$

$$Fr = \frac{V}{\sqrt{gL}} \tag{28}$$

where, V and L are forward velocity and length of the ship, respectively.

$$\lambda = \frac{L_S}{L_m} \tag{29}$$

Here, λ is the scale factor. The dynamic similarity between the model and full-scale can be satisfied by either Reynolds or Froude numbers. Froude similarity is used for the surface type vessels in which the wave resistance can be significant, and gravity-induced forces are dominant. On the other hand, Reynolds similarity is preferred for submerged vessels moving in a depth in which the free surface effects are neglected, and viscous effects are dominant. According to these two dynamic similarities, the kinematic similarity between model and full scale can be obtained as given below;

$$\frac{V_M L_M}{\vartheta_M} = \frac{V_S L_S}{\vartheta_S} \rightarrow V_S = \frac{V_m}{\lambda} \, (Re\ Similarity) \tag{30}$$

$$\frac{V_S}{\sqrt{g_S L_S}} = \frac{V_M}{\sqrt{g_M L_M}} \rightarrow V_S = V_M \sqrt{\lambda}\ (Fr\ Similarity) \quad (31)$$

As can be seen in Equation 30, when the Re similarity is satisfied between the model and full scale, the model scale velocities exceed the practical speed limitations of the experimental facilities. The model tests of the submarine form (i.e., Model 1) was conducted at five different velocities from 3.051m/s to 9.152 m/s in the David Taylor Model Basin [38–40]. Although the Re similarity is expected to be used for fully submerged bodies, in our case, the full-scale velocities become unrealistic with the application of the Re similarity as given in Table 4. For this reason, Fr similarity is considered to be more suitable to find the full-scale velocities. However, when the Fr similarity is satisfied, the full-scale submarine velocities still remain in an unrealistic speed range, as shown in Table 4. Therefore, in this study, the two different velocities (i.e., V_S= 13.472m/s and 14.947m/s) obtained by Fr similarity were used to investigate the scale effects, whereas the realistic submarine velocities (i.e., from 10 knots to 29 knots) were used to predict the self-propulsion characteristics in full-scale.

Table 4. *The change in full-scale submarine velocities with the Reynolds and Froude similarities.*

V_{M1} (m/s)	V_S (m/s) (Re Similarity)	V_S (m/s) (Fr Similarity)
2.750	0.115	13.472
3.051	0.127	14.947
5.144	0.214	25.200
6. 096	0.254	29.864
7.161	0.298	35.082
8.231	0.348	40.324
9.152	0.381	44.835

5.2.1. Validation of Total Resistance for Model 1

The total resistance of the model scale submarine form (i.e., λ=24) was validated with the available experimental data [40]. The experimental data was obtained by conducting the wind tunnel and towing tank tests. During the experiments, the mean velocities and turbulence intensities were measured in the wind tunnel tests. On the other hand, the towing tank tests were conducted to measure the total resistance of the submarine forms. The details about the wind tunnel and towing tanks tests can be found in the technical reports (e.g., [38,40]). Figure 9 shows the comparison of experiment and numerical data regarding total resistance for Model 1 (i.e., λ=24). As shown in Figure 9, there is a good agreement between CFD and the experimental data. The absolute relative difference between the CFD prediction and the experimental values was found a maximum of 7%.

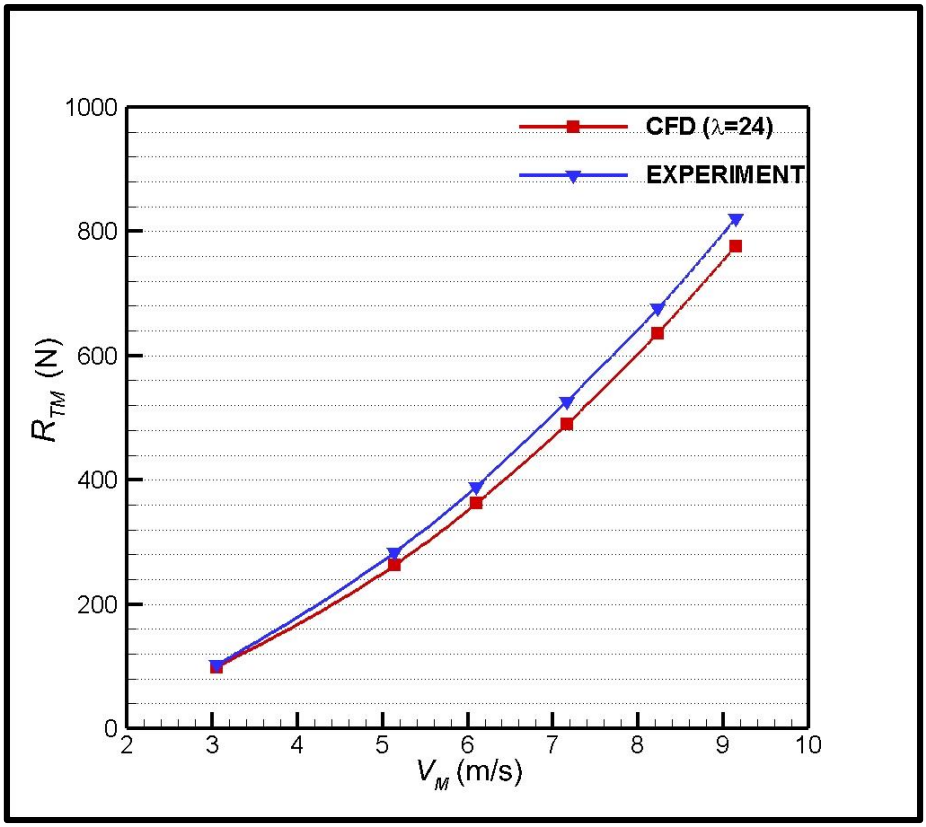

Figure 9. *Validation of model scale resistance analyses for Model 1 (λ=24).*

5.2.2. Validation of skin friction coefficients (C_F) with the ITTC-1957 correlation line for the full-scale submarine

Figure 10 compares the frictional resistance coefficients obtained from the CFD and ITTC-1957 correlation line for the full-scale submarine form between 10knots and 29knots. In general, the full-scale CFD simulations' accuracy might be evaluated with the summation of residual resistance obtained by the model experiments, numerical methods or empirical formulations, and frictional resistance computed by the ITTC-1957 correlation line for the surface ships. Then, the total resistance can be compared with those of full-scale CFD results. The reason is that the residual resistance coefficient is assumed to be constant with the change in scale ratio. However, in our case, residual resistance only comprises the viscous pressure resistance, which constitutes a small portion of residual resistance, and it is not constant with the scale ratio. As there is no numerical data for the full-scale submarine form to compare the present CFD results, the numerical results were compared with the ITTC-1957 correlation line in terms of the skin friction coefficient at varying forward speeds. It should be noted that, although the ITTC-1957 correlation line is an empirical formulation, its reliability is shown with different studies in the literature for the frictional resistance prediction of the surface ships. As the boundary layer's realistic solution is strongly related to frictional force prediction, the comparison of the skin friction coefficients obtained by the CFD and ITTC-1957 correlation line proves

the boundary layer resolution's accuracy in full-scale CFD simulations. As shown in Figure 10, the absolute relative differences between the two approaches were found between 1% and 2%.

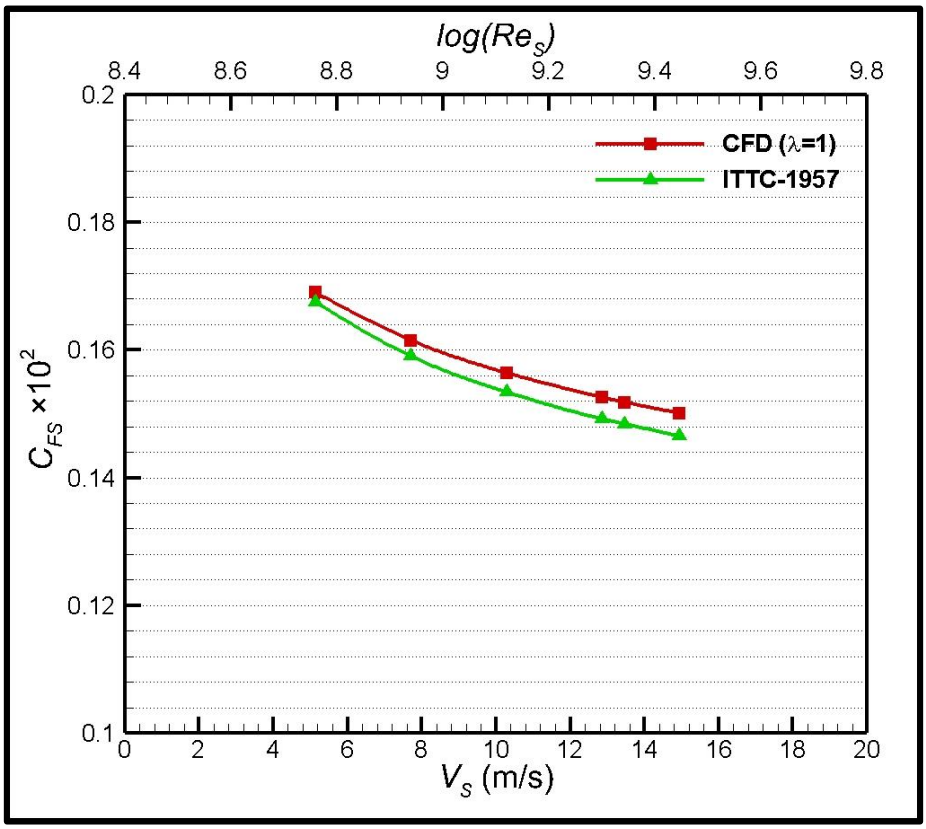

Figure 10. *Comparison of the skin friction coefficients obtained by CFD and ITTC-1957 correlation line for the full-scale submarine form.*

5.3. Self-propulsion analysis in model scale for Model 1 (λ=24)

In the self-propulsion tests, the hull forwards with its propeller at the desired speed. Hence, the thrust, torque, and propeller rotational rates are measured in the self-propulsion tests. In this study, the predicted self-propulsion performance characteristics are compared with the experimental data and other numerical studies in the literature for Model 1 (λ=24) at V_M=2.75 m/s as shown in Table 5. In these studies, the contribution of skin friction correction force (F_D), which is the external tow force applied to the model hull to impose the full-scale self-propulsion point, was neglected. In the study of Ozden et al., [31], the self-propulsion tests were performed for the model scale DARPA Suboff form (i.e., Model 1, λ=24) by using the load variation method for constant speed and seven different propeller rotational rates. The details about the experiments can be found in Ozden et al., [31]. In our previous study [29], the self-propulsion characteristics of the model scale submarine form (i.e., λ=24) were investigated comprehensively using both the actuator disc and discretised propeller techniques for a wide range of forward speeds. In this study, CFD simulations were first conducted in free-running self-propelled conditions for Model 1 to compare the numerical results with the experiment and other numerical studies in the literature. Following this, the skin friction correction force (i.e., F_D) was taken

into account to extrapolate the results from the model to full-scale using the 1978 ITTC method. In this way, the full-scale CFD results were compared with the predictions using the 1978 ITTC method. Table 5 shows the comparison of non-dimensional thrust and torque coefficients computed at the self-propulsion point and 2.75 m/s. The numerical results, which were obtained by taking F_D into account, are also presented in Table 5. As shown in the table, the thrust and torque coefficients in the self-propelled case agree with the other numerical studies in the literature. However, similar to those numerical studies, the thrust and torque coefficients were underpredicted by the CFD compared to the experimental data. Also, it is clear that the thrust and torque coefficients decrease with the application of F_D.

Table 5. *Comparison of propeller characteristics in the self-propelled case at V_{M1}=2.75 m/s and Model 1 (λ=24)*

Numerical/Experimental Studies (Self-Propelled Case)	K_T	K_Q
Chase and Carrica [27] (CFD) - w/o F_D	0.2342	0.0471
Kinaci et al. [47] (CFD) - w/o F_D	0.2312	-
Ozden et al. [31] (CFD) - w/o F_D	0.2417	0.0463
Ozden et al. [31] (EFD) - w/o F_D	0.2751	0.0561
Sezen et al. [29] (CFD) - w/o F_D	0.2363	0.0456
Present study- w/o F_D	0.2342	0.0452
Present study- w/ F_D	0.1864	0.0395

5.4. Investigation of scale effects on hydrodynamic characteristics

5.4.1. Scale effects on resistance

The scale effects on the resistance components in bare hull condition were investigated at two different velocities using the Fr similarity in Table 6. As shown in this table, the total resistance and viscous pressure resistance coefficients change with an increase in the model length and Reynolds number. The different eddy structure around the submarine forms causes a variation of the pressure fields at the submarine aft-end. Thus, the non-dimensional viscous pressure coefficients are predicted alternatively.

Table 6. *Scale effects on total resistance and viscous pressure coefficients at two different forward speeds.*

λ	1		2		24	
V(m/s)	13.472	14.947	9.526	10.569	2.750	3.051
Re	$1.288*10^9$	$1.429*10^9$	$4.555*10^8$	$5.053*10^8$	$1.096*10^7$	$1.216*10^7$
C_T	$1.990*10^{-3}$	$1.971*10^{-3}$	$2.230*10^{-3}$	$2.207*10^{-3}$	$3.399*10^{-3}$	$3.354*10^{-3}$
C_{VP}	$4.717*10^{-4}$	$4.694*10^{-4}$	$4.911*10^{-4}$	$4.884*10^{-4}$	$6.252*10^{-4}$	$6.185*10^{-4}$

5.4.2. Scale effects on nominal wake

The nominal wake characterises the mean inflow velocity at the propeller plane in the absence of the propeller. The mean velocity field at the propeller plane is affected by the flow around the hull and

the appendages near the propeller plane; thus, it changes in axial, tangential and radial directions. The wake field's accurate estimation at the propeller plane is vital for the wake adapted propeller design. The nominal wake fraction of a ship can be divided into three components [58].

$$w = w_p + w_f + w_w \tag{32}$$

Here, w_p is the potential wake, w_f is the frictional wake fraction and w_w is the wave component of the wake fraction. The potential wake field occurs if the vessel operates in an ideal fluid. In general, the potential wake fraction is a small component of the total wake fraction, and it can be calculated using the analytical methods [58]. The wake fraction's wave component occurs due to the orbital actions of the water particles on the water surface. As the submarine form is assumed fully submerged, the wave component can be ignored in this study. The frictional wake fraction is the major contributor to the total wake fraction. Since the velocities are different in the boundary layer between model and full-scale, the frictional wake fraction changes significantly in full-scale compared to the model scale [59].

The nominal wake field data is generally characterised by Taylor's wake fraction, and it can be defined as follows:

$$w_n = \frac{V_S - V_A}{V_S} \tag{33}$$

where V_A is the advance velocity in the axial direction at the propeller plane.

Figure 11 shows the non-dimensional axial velocity distributions at the propeller plane (i.e., x/L=0.978) and two different velocities (i.e., corresponding to 26knots and 29kots in full-scale) for each scale. As it can be clearly observed in Figure 11, the V-shaped carving (wake shadow) at the 12 o'clock position is caused by the sail for all scales. As expected, the boundary layer is thinner in full-scale than in model scales, and the low-velocity region is more pronounced in model scales at the propeller plane. The boundary layer formation in full-scale enables higher wake velocities at the propeller plane compared to the model scale. Also, it is clear from Figure 11 that the wake velocities increase with a decrease in scale ratio that results in reduced nominal wake fraction value in full scale due to the scale effects associated with the Re number and boundary layer formation (i.e., thinner boundary layer). It is to be noted that the hub to propeller diameter ratio (D_{hub}/D) was set to 0.226.

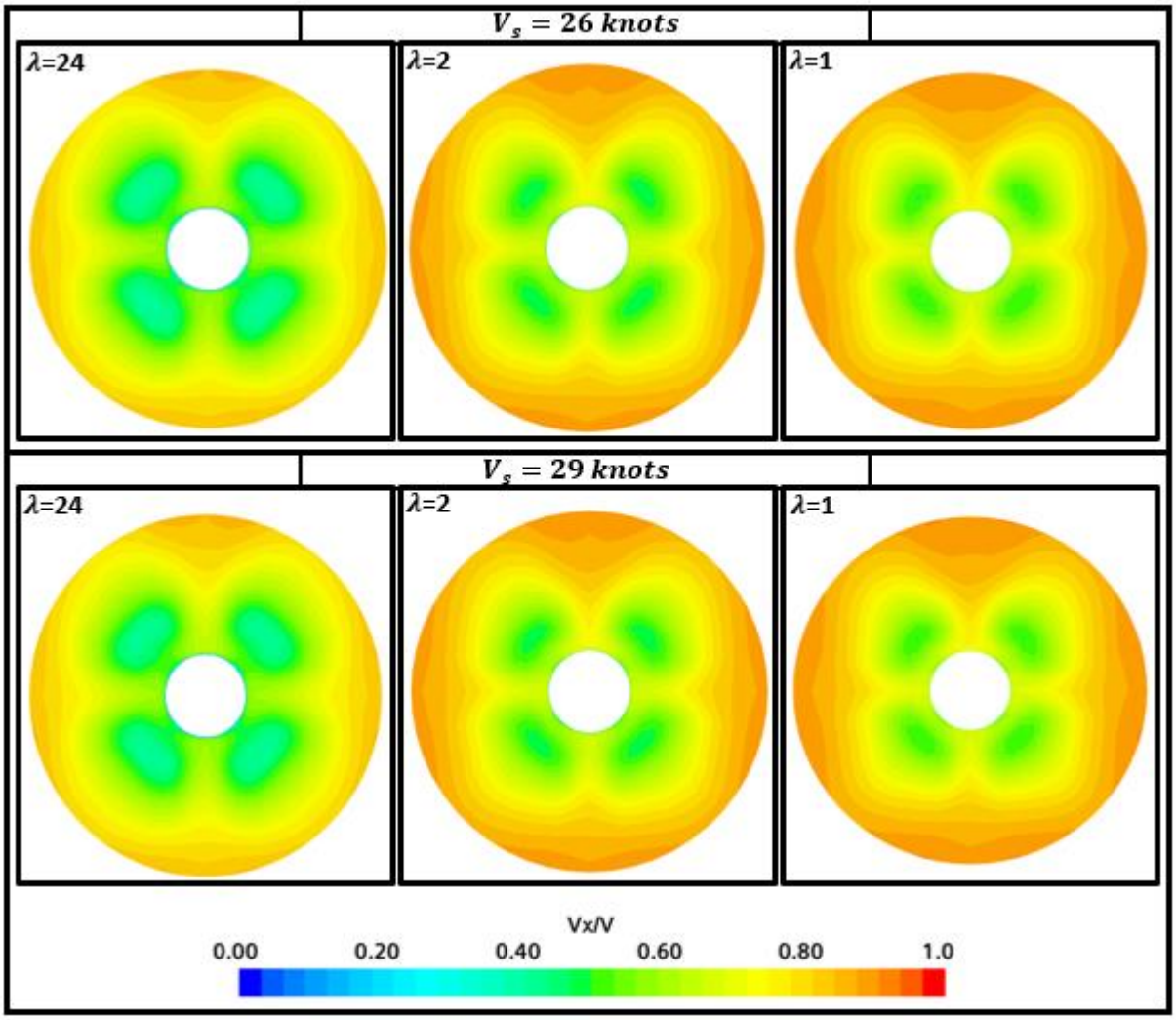

Figure 11. *Comparison of the non-dimensional axial velocity distributions at two different velocities and x/L=0.978 (Top: corresponding 26knots in full scale, Bottom: corresponding 29knots in full-scale).*

Table 7 lists the computed mean value of the nominal wake fraction at the propeller plane for each scale ratio corresponding to 26knots and 29knots in full-scale. As shown in this table, the nominal wake fraction values decrease with an increase in Re number and a decrease in scale ratio.

Table 7. *Scale effects on nominal wake fraction at two different forward speeds.*

λ	1		2		24	
V(m/s)	13.472	14.947	9.526	10.569	2.750	3.051
Re	$1.288*10^9$	$1.429*10^9$	$4.555*10^8$	$5.053*10^8$	$1.096*10^7$	$1.216*10^7$
w_n	0.233	0.231	0.255	0.253	0.341	0.338

Additionally, the nominal wake fractions are shown in Figure 12 at varying velocities for the full-scale submarine form. As shown in Figure 12, the nominal wake fraction values decrease with an increase in the vessel's forward speeds.

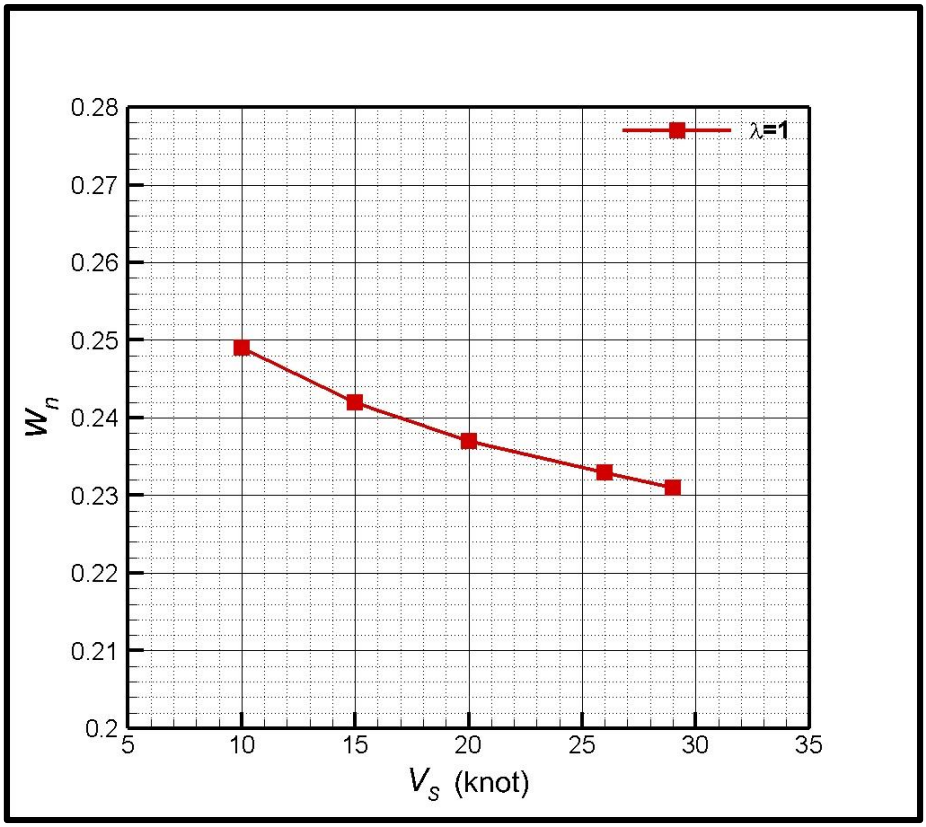

Figure 12. *Comparison of the nominal wake fractions at various velocities for λ=1.*

5.4.3. Scale effects on self-propulsion characteristics

In the self-propulsion simulations, F_D can be included in the calculations for the model scales according to the following formulation;

$$F_D = \frac{1}{2}\rho_M S_M {V_M}^2 (C_{FM} - C_{FS}) \tag{34}$$

Here, subscript M and S denote the model and full-scale submarine, respectively. S is the wetted surface area, (m^2); and V_M is the submarine velocity, m/s [60,61]. In this study, the self-propulsion simulations were conducted to find the self-propulsion point using the PI controller. At the self-propulsion point, the thrust identity method was applied to find the self-propulsion characteristics (i.e., propeller-hull interaction or propulsive coefficients) using the open water curve of each propeller scale, which is obtained by the CFD simulations. Table 8 and 9 show the propulsive coefficients at 26knots and 29knots, respectively. As given in Table 8 and 9, the effective wake fraction decreases with a decrease in the scale ratios. The reason behind this is that the frictional coefficient reduces with an increase in Re number. The increase in inflow velocity results in a reduction of the propeller loading; thus, the advance ratio increases. As well as the effective wake fraction and the thrust deduction, the non-dimensional thrust, torque coefficients and hull efficiency decrease with an increase in model length at both forward speeds. However, the relative-rotative efficiency does not show the same trend with a decrease in the scale ratio compared to other self-propulsion

characteristics. This can be related to the different prediction of the torque coefficients in open water simulations as the torque coefficient is more dependent on the scale effects than those of the thrust coefficients (see Figure 8) [22]. The differences in the relative rotative efficiency caused deterioration of the trend in the propulsive efficiency.

Table 8. *Self-propulsion characteristics for each scale corresponding to 26knots in full-scale.*

λ	1	2	24
V (knots)	26.189	18.519	5.346
n(rps)	1.739	2.430	8.067
K_T	0.163	0.170	0.186
$10K_Q$	0.324	0.334	0.383
t	0.144	0.145	0.209
J	0.913	0.885	0.840
w	0.259	0.290	0.355
η_0	0.732	0.716	0.649
η_H	1.156	1.204	1.226
η_R	0.953	0.942	0.974
η_D	0.807	0.812	0.775

Table 9. *Self-propulsion characteristics for each scale corresponding to 29knots in full-scale.*

λ	1	2	24
V (knots)	29.057	20.549	5.931
n(rps)	1.924	2.693	8.991
K_T	0.162	0.169	0.188
$10K_Q$	0.323	0.332	0.386
t	0.144	0.145	0.209
J	0.914	0.887	0.836
w	0.260	0.289	0.355
η_0	0.733	0.719	0.648
η_H	1.157	1.203	1.226
η_R	0.952	0.942	0.974
η_D	0.808	0.815	0.774

5.5. Full-scale resistance and self-propulsion prediction with the 1978 ITTC method

5.5.1. Extrapolation of total resistance

Table 10 shows the comparison of the full-scale CFD predictions and extrapolated results using both Froude and Hughes extrapolation methods (i.e., 1957 and 1978 ITTC procedures) in terms of total resistance coefficients at two different forward speeds. In the modified Hughes approach (i.e., 1978 ITTC), the form factor was taken into account, whereas the C_{vp} coefficient was assumed constant at both model and full-scale submarine hull forms in the Froude approach. As shown in Table 10, the Froude approach gives better results than those of Hughes approach. This is because the submarine hull form operates a relatively high Fr number (i.e., Fr=0.42 and 0.47). Hence, the Froude approach is more suitable than the 1978 ITTC procedure for extrapolating the total resistance from the model to the full-scale at the specified operating conditions. Also, the difference between the CFD predictions and extrapolated results reduces with a decrease in the scale ratio in both methods.

Table 10. *Comparison of total resistance coefficients at two different velocities in full-scale.*

	V_S *(knots)*	C_{TS}*10^3 *CFD* (λ=1)	λ=2	$\%\Delta C_{TS}$ (λ=2)	λ=24	$\%\Delta C_{TS}$ (λ=24)
1957 ITTC procedure (Froude Method)	26	1.990	1.975	0.754	2.109	5.980
	29	1.971	1.953	0.913	2.083	5.682
1978 ITTC procedure (Modified Hughes Method)	26	1.990	1.903	4.372	1.818	8.643
	29	1.971	1.881	4.617	1.796	8.879

5.5.2. Extrapolation of self-propulsion characteristics

Here, the equations used to determine the self-propulsion characteristics of the submarine hull forms are given briefly. Propeller advance coefficient (J_T) and torque coefficient (K_{QT}) obtained by thrust identity are read off from the open water diagram of the model propeller. The wake fraction (w_T) at model scale is then calculated as follows:

$$w_T = 1 - \frac{J_T D n}{\mathrm{V}} \tag{35}$$

the relative rotative efficiency (η_R) is expressed as the ratio of the torque coefficients generated by the propeller in open water (K_{QT}) to behind the hull conditions (K_Q).

$$\eta_R = \frac{K_{QT}}{K_Q} \tag{36}$$

The thrust deduction factor (t) can be described as follows:

$$t = \frac{T + F_D - R_T}{T} \tag{37}$$

where, T is the thrust force generated by the propeller at the self-propulsion point and R_T is the bare hull resistance without propeller.

Following the procedure described by ITTC [21], the scale effect correction can be implemented using Equation (38) based on the model-based data and hence the full-scale wake fraction can be determined.

$$w_{TS} = (t + w_R) + (w_{TM} - t - w_R)\frac{(1+k)C_{FS} + \Delta C_F}{(1+k)C_{FM}} \tag{38}$$

where w_R is the rudder effect on the wake fraction and ΔC_F is the roughness effect. In this study, w_R was taken 0.04 as recommended in the ITTC guideline [21] and roughness coefficient was neglected as the submarine forms were assumed in smooth condition. The full-scale propeller load can be derived as below;

$$\frac{K_{TS}}{{J_S}^2} = \frac{1}{N_P}\frac{S_S}{2{D_S}^2}\frac{C_{TS}}{(1-t)(1-w_{TS})^2} \tag{39}$$

where N_P is the number of propellers (i.e., in our case N_P=1). Using the ${K_{TS}}/{J_S}^2$ value, the full-scale advance coefficients (J_{TS}) and the torque coefficient (K_{QS}) are read off from the numerical results of full-scale propeller characteristics.

The propeller rotational speed and other required self-propulsion characteristics for the full-scale submarine are determined by using the following equations [21]:

- The propeller rate of revolution:

$$n_S = \frac{(1 - w_{TS})V_S}{J_{TS}D_S} \tag{40}$$

- The thrust of a propeller:

$$T_S = (K_{TS}/J_S^2)J_{TS}^2\,\rho_S D_S^4 n_S^2 \tag{41}$$

- The torque of a propeller:

$$Q_S = \left(K_{QTS}/\eta_R\right)\rho_S D_S^5 n_S^2 \tag{42}$$

- The delivered power of a propeller

$$P_{DS} = 2\pi Q_S n_S \tag{43}$$

- The effective power:

$$P_E = R_{TS}V_S \tag{44}$$

- The hull efficiency:

$$\eta_H = \frac{1 - t}{1 - w_{TS}} \tag{45}$$

- The propulsive efficiency:

$$\eta_D = \frac{P_E}{P_{DS}} \tag{46}$$

Based on the determined propulsion characteristics, Figure 13 shows the comparison between the full-scale predictions from the CFD and the 1978 ITTC performance prediction method at 26knots and 29knots. With a decrease in the scale ratio, the differences between the CFD prediction and extrapolated results reduce considerably, particularly for the thrust deduction factor and the torque coefficient. In the 1978 ITTC method, the thrust deduction factor is assumed to be constant both in the model and full-scale; hence, the correction is not applied to extrapolate the thrust deduction factor from the model scale to full-scale [21, 62]. However, the numerical results show that the thrust

deduction factor is affected by the scale ratio variation compared to the full-scale CFD predictions. As shown in Figure 13, Table 8 and 9, the scale effects become negligible for the thrust deduction factor when the scale ratio is reduced. Also, the different prediction of the thrust deduction factor causes deterioration of the trend for the hull efficiency values between the extrapolated data and CFD prediction. The self-propulsion point (i.e., propeller rotational speed) and thrust coefficient are estimated with good accuracy using two models' extrapolated data with the aid of the 1978 ITTC method compared to full-scale CFD prediction. However, similar to the thrust deduction factor, the discrepancy for predicting the torque coefficient increases between the CFD prediction and extrapolated data with an increase in scale ratio. Akin to another numerical study conducted by the RANS solver [24], the difference between the extrapolated data and CFD prediction is found relatively high for predicting the torque coefficient using the 1978 ITTC method when the scale ratio is increased. Although the 1978 ITTC method generally predicts the self-propulsion characteristics with good accuracy, the alternative prediction of thrust deduction factor and torque coefficients, particularly for the extrapolation of results using Model 1, causes deterioration of the trend for the relative rotative efficiency and hull efficiency compared to the other self-propulsion characteristics (e.g., effective wake, open water propeller efficiency, propulsive efficiency and delivered power). Therefore, the 1978 ITTC method might not be adequate to extrapolate the model's torque coefficient to full-scale if the scale ratio is high. Also, the assumption of the same thrust deduction factor might be another deficiency of the 1978 ITTC method when the scale ratio increases considerably. It should be noted that the self-propulsion characteristics are included in the Appendix (Table A.1–A.2).

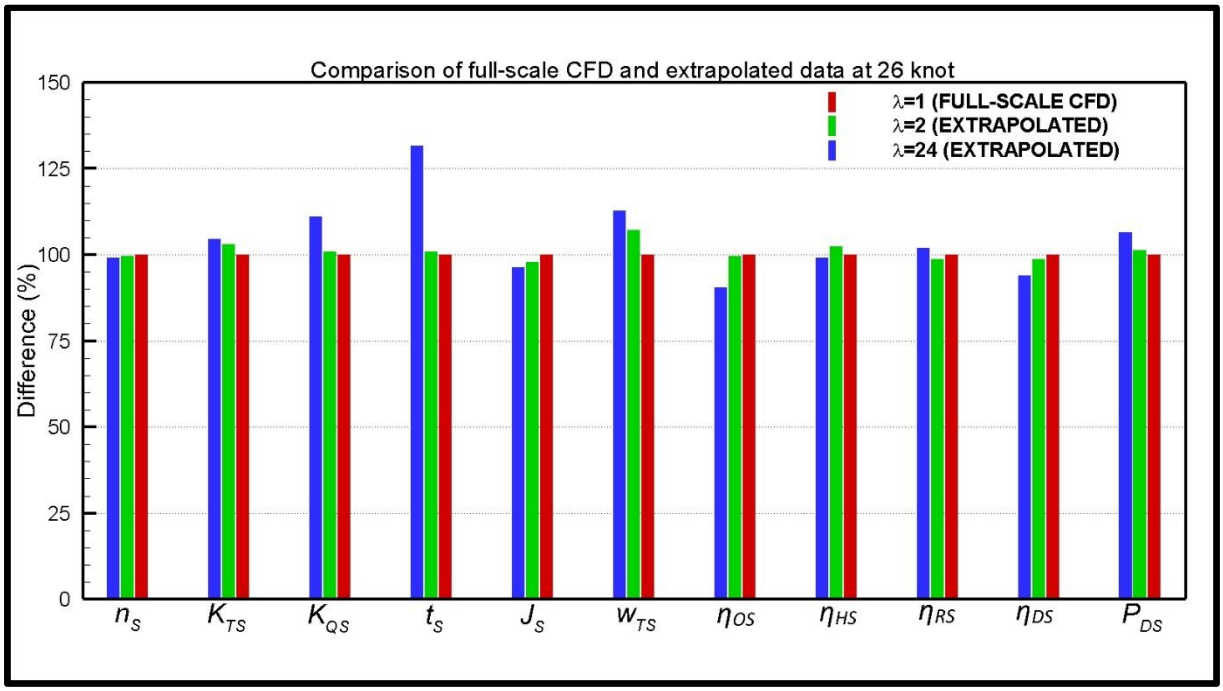

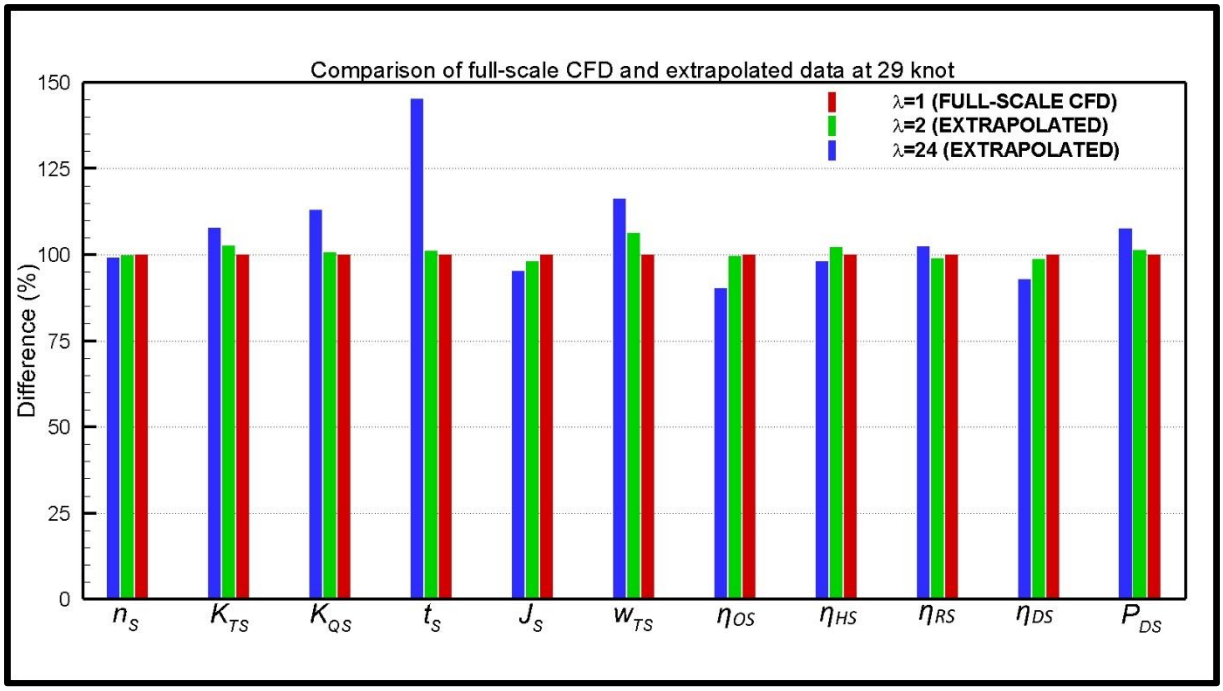

Figure 13. *Comparison of full-scale CFD results and extrapolated results using 1978 ITTC performance prediction method at two different velocities (*Here, 100% is the full-scale CFD results).

5.6. Calculation of self-propulsion characteristics in full-scale using CFD

In this section, further numerical analyses were conducted in full-scale to predict the DARPA Suboff form's self-propulsion characteristics for a wide range of representative forward speeds, as stated in Section 5.2, using the open water propeller data obtained by the CFD. As shown in Table 11, the self-propulsion characteristics are found independent of the forward speed. Thus, the prediction of the self-propulsion characteristics at one of the forward velocities enables the prediction of the self-propulsion characteristics for the desired forward speeds. Figure 14A and 14B shows the change in the self-propulsion points and delivered power with the forward speed. As expected, the delivered power and self-propulsion points increase with an increase in the forward speed. The relationship between the self-propulsion point and forward speed is linear. As shown in Figure 14B, the service speed of the full-scale submarine can be considered around 25knots.

Table 11. *Self-propulsion characteristics at various forward speeds in full-scale.*

V (knots)	10.0	15.0	20.0	25.0	26.189	29.057
n(rps)	0.677	1.008	1.336	1.662	1.739	1.924
K_T	0.172	0.168	0.165	0.163	0.163	0.162
$10K_Q$	0.335	0.330	0.326	0.324	0.324	0.323
$1-t$	0.859	0.858	0.857	0.857	0.856	0.856
J	0.895	0.903	0.908	0.912	0.913	0.914
$1-w$	0.741	0.742	0.742	0.741	0.741	0.740
η_0	0.729	0.731	0.732	0.732	0.732	0.733
η_H	1.159	1.156	1.155	1.156	1.156	1.157
η_R	0.959	0.957	0.956	0.954	0.953	0.952
η_D	0.810	0.809	0.808	0.808	0.807	0.808
P_D (kW)	670.714	2177.970	5025.624	9612.280	11003.655	14878.373

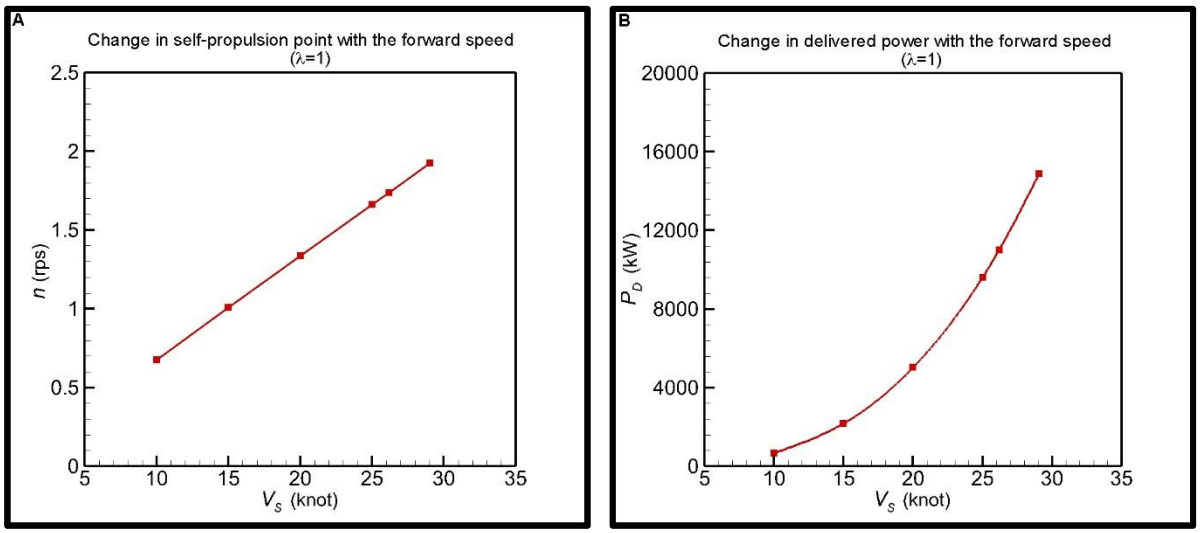

Figure 14. *Change in self-propulsion points (A) and delivered power (B) with the forward speed (λ=1).*

5.7. Concluding Remarks

The 1978 ITTC Performance prediction method was established and recommended to predict the full-scale powering performance of single screw surface ships based on model test data by extrapolation. Over the years, this method was also extended for the power prediction of other ship types, e.g., catamarans etc., due to practical reasons for the power prediction in the preliminary design stage. Within the same context, however, the feasibility of this method has not been explored yet for the power prediction of submerged vessels (e.g., submarines). Also, while it is difficult to find any published powering performance data for a full-scale submarine in the open literature, there are some published useful data in model scale for the widely used benchmark DARPA Suboff hull form which may represent a typical submarine hull form.

It has also become clear that, in recent years, with the further development of computational methods and computing resources, the accuracy and usage of the CFD methods for the performance prediction of the model and full-scale ships have been proven by several studies in the literature. This development is also coupled with the inherent advantage of the CFD methods for better modelling the physics of the power prediction problem independent of the scale effects in the model and full-scale.

Within the above framework, to achieve the aim of this paper, the state of art commercial CFD tool was applied to DARPA Suboff hull form. For this purpose, three DARPA Suboff hull forms with varying scale ratios were generated, one of them being a full-scale representative submarine, and the flow around these forms was solved to predict the resistance, self-propulsion, and open water propeller performance characteristics using CFD. In this way, the scale effects on the resistance, nominal wake

and self-propulsion characteristics were investigated, and the results were presented and discussed in Section 5. 4 as one of the aims of this study.

Following the scale effect investigation, the performance prediction of the full-scale (DARPA) submarine form was conducted by using the model scale data, which were created by the CFD, with the aid of the 1978 ITTC method, for the first time, to achieve the other aim of this study. The predicted results from the 1978 ITTC method were compared with the direct CFD predictions in full-scale, and results were presented and discussed in Section 5.5. Additionally, for practical use purpose, the full-scale self-propulsion performance characteristics of the DARPA Suboff hull form were presented and discussed in Section 5.6 over a realistic forward speed range of a submarine for the first time.

Based on the above summarised numerical investigations, which were validated with model test data available in the open literature, the authors believe that this study presented a valuable contribution to the performance prediction of submarines and associated scale effects that can be very useful in the preliminary design stage of these submarines.

6. Conclusions

In this study, using CFD methods and the benchmark DARPA Suboff hull form, the scale effects on the resistance, nominal wake and self-propulsion characteristics of submarines were investigated, including a representative full-scale submarine based on the DARPA Suboff. Also, the applicability of the 1978 ITTC performance prediction method was explored for the submarines for the first time. Based on these investigations, the following main conclusions were found:

- The total, frictional and viscous pressure resistance coefficients decreased with an increase in scale ratios and associated Re numbers. Hence, the total resistance coefficients of the model scale submarine forms were higher than those of the full-scale submarine due to the different flow regimes caused by the different *Re* numbers.
- The total resistance coefficients of the full-scale submarine form obtained by the CFD computations were compared with the extrapolated data using the Froude and Hughes approaches at two different forward speeds. As the submarine velocities are relatively high and wave resistance is neglected, the Froude approach presented better correlations with the CFD predictions compared to the Hughes approach for the total resistance in the full-scale.
- The comparison of the nominal wake velocities at the propeller plane (i.e., x/L=0.978) showed that the velocities were higher in full-scale in comparison with the model scales due to the differences both in *Re* number and the boundary layer structure between the model and full-scale. This consequently resulted in smaller nominal wake fraction values in full-scale.

- The self-propulsion results belong to different model scales indicated that with an increase in the model length, the scale effects on the self-propulsion characteristics would be reduced.
- Although the 1978 ITTC performance prediction method is mainly recommended for surface ships and its application to submerged bodies may be questionable, this study indicated that this method could be used in some confidence for submarines for practical purposes in the preliminary design stage.

Acknowledgements

The first author is sponsored by Stone Marine Propulsion Ltd of the UK and the University of Strathclyde during his PhD study. Results were obtained using the ARCHIE-WeSt High-Performance Computer (www.archie-west.ac.uk) based at the University of Strathclyde. The authors would like to thank Francesco Salvatore from INSEAN for providing the 3-D geometry and experimental data of E1619 propeller.

References

[1] W. Sun, Q. Hu, S. Hu, J. Su, J. Xu, J. Wei, G. Huang, Numerical Analysis of Full-Scale Ship Self-Propulsion Performance with Direct Comparison to Statistical Sea Trail Results, J. Mar. Sci. Eng. 8 (2020) 24. https://doi.org/10.3390/jmse8010024.

[2] H. Jasak, V. Vukčević, I. Gatin, I. Lalović, CFD validation and grid sensitivity studies of full scale ship self propulsion, Int. J. Nav. Archit. Ocean Eng. 11 (2019) 33–43. https://doi.org/10.1016/j.ijnaoe.2017.12.004.

[3] V. Bertram, Practical Ship Hydrodynamics, 2nd ed., Elsevier Science, 2014.

[4] L. Larsson, F. Stern, M. Visonneau, eds., Numerical Ship Hydrodynamics, Springer Netherlands, Dordrecht, 2014. http://link.springer.com/10.1007/978-94-007-7189-5.

[5] D. Ponkratov, Lloyd's Register workshop on ship scale hydrodynamics, in: UK, 2016.

[6] D. Ponkratov, C. Zegos, Validation of ship scale CFD self-propulsion simulation by the direct comparison with sea trials results, Fourth International Symposium on Marine Propulsors, Austin, Texas, USA, 2015.

[7] H. Mikkelsen, J.H. Walther, Effect of roughness in full-scale validation of a CFD model of self-propelled ships, Appl. Ocean Res. 99 (2020) 102162. https://doi.org/10.1016/j.apor.2020.102162.

[8] M. Terziev, T. Tezdogan, A. Incecik, A geosim analysis of ship resistance decomposition and scale effects with the aid of CFD, Appl. Ocean Res. 92 (2019) 101930. https://doi.org/10.1016/j.apor.2019.101930.

[9] A. Dogrul, S. Song, Y.K. Demirel, Scale effect on ship resistance components and form factor, Ocean Eng. 209 (2020) 107428. https://doi.org/10.1016/j.oceaneng.2020.107428.

[10] Q. Zeng, R. Hekkenberg, C. Thill, H. Hopman, Scale effects on the wave-making resistance of ships sailing in shallow water, Ocean Eng. 212 (2020) 107654. https://doi.org/10.1016/j.oceaneng.2020.107654.

[11] C. Delen, S. Bal, Telfer's Geosim Method Revisited by CFD, Int. J. Marit. Eng. 161 (2019). https://doi.org/10.3940/rina.ijme.2019.a4.563.

[12] P.M. Carrica, H. Fu, F. Stern, Computations of self-propulsion free to sink and trim and of motions in head waves of the KRISO Container Ship (KCS) model, Appl. Ocean Res. 33 (2011) 309–320. https://doi.org/10.1016/j.apor.2011.07.003.

[13] Z. Shen, D. Wan, P.M. Carrica, Dynamic overset grids in OpenFOAM with application to KCS self-propulsion and maneuvering, Ocean Eng. 108 (2015) 287–306. https://doi.org/10.1016/j.oceaneng.2015.07.035.
[14] S. Gaggero, D. Villa, M. Viviani, An extensive analysis of numerical ship self-propulsion prediction via a coupled BEM/RANS approach, Appl. Ocean Res. 66 (2017) 55–78. https://doi.org/10.1016/j.apor.2017.05.005.
[15] D. Villa, S. Gaggero, T. Gaggero, G. Tani, G. Vernengo, M. Viviani, An efficient and robust approach to predict ship self-propulsion coefficients, Appl. Ocean Res. 92 (2019) 101862. https://doi.org/10.1016/j.apor.2019.101862.
[16] A.M. Castro, P.M. Carrica, F. Stern, Full scale self-propulsion computations using discretized propeller for the KRISO container ship KCS, Comput. Fluids. 51 (2011) 35–47. https://doi.org/10.1016/j.compfluid.2011.07.005.
[17] V. Vukcevic, H. Jasak, I. Gatin, T. Uroic, Ship Scale Self Propulsion CFD Simulation Results Compared to Sea Trial Measurements, VII International Conference on Computational Methods in Marine Engineering, Nantes, France, 2017.
[18] B. Starke, J. Bosschers, Analysis of scale effects in ship powering performance using a hybrid RANS-BEM approach, 29th Symposium on Naval Hydrodynamics, Gothenburg, Sweden, 2012.
[19] A. Farkas, N. Degiuli, I. Martić, Assessment of hydrodynamic characteristics of a full-scale ship at different draughts, Ocean Eng. 156 (2018) 135–152. https://doi.org/10.1016/j.oceaneng.2018.03.002.
[20] ITTC, Report of Resistance Committee, Madrid, 1957.
[21] ITTC, 7.5-02-03-01.4 1978 ITTC Performance Prediction Method, ITTC - Recomm. Proced. Guidel., 2017.
[22] T.-Y. Lin, J.-S. Kouh, On the scale effect of thrust deduction in a judicious self-propulsion procedure for a moderate-speed containership, J. Mar. Sci. Technol. 20 (2015) 373–391. https://doi.org/10.1007/s00773-014-0289-7.
[23] D. Zhao, C. Guo, J. Lin, Z. Zhang, X. Bai, Prediction of Self-Propulsion Performance of Ship Model with Double L-Type Podded Propulsors and Conversion Method for Full-Scale Ship, J. Mar. Sci. Eng. 7 (2019) 162. https://doi.org/10.3390/jmse7050162.
[24] C. Delen, U. Can, S. Bal, Prediction of Resistance and Self-Propulsion Characteristics of a Full-Scale Naval Ship by CFD-Based GEOSIM Method, J. Ship Res. (2020) 16. http://dx.doi.org/10.5957/JOSR.03200022.
[25] M. Renilson, Submarine Hydrodynamics, 2nd edition, Springer, 2018.
[26] N. Chase, Simulations of the DARPA Suboff submarine including self-propulsion with the E1619 propeller, Master Thesis, University of Iowa, 2012.
[27] N. Chase, P.M. Carrica, Submarine propeller computations and application to self-propulsion of DARPA Suboff, Ocean Eng. 60 (2013) 68–80. https://doi.org/10.1016/j.oceaneng.2012.12.029.
[28] N. Zhang, S. Zhang, Numerical simulation of hull/propeller interaction of submarine in submergence and near surface conditions, J. Hydrodyn. 26 (2014) 50–56. https://doi.org/10.1016/S1001-6058(14)60006-8.
[29] S. Sezen, A. Dogrul, C. Delen, S. Bal, Investigation of self-propulsion of DARPA Suboff by RANS method, Ocean Eng. 150 (2018) 258–271. https://doi.org/10.1016/j.oceaneng.2017.12.051.
[30] A. Posa, E. Balaras, Large-Eddy Simulations of a notional submarine in towed and self-propelled configurations, Comput. Fluids. 165 (2018) 116–126. https://doi.org/10.1016/j.compfluid.2018.01.013.
[31] Y.A. Özden, M.C. Özden, E. Demir, S. Kurdoglu, Experimental and Numerical Investigation of DARPA Suboff Submarine Propelled with INSEAN E1619 Propeller for Self-Propulsion, J. Ship Res. 63 (2019) 235–250.
[32] P.M. Carrica, Y. Kim, J.E. Martin, Near-surface self propulsion of a generic submarine in calm water and waves, Ocean Eng. 183 (2019) 87–105. https://doi.org/10.1016/j.oceaneng.2019.04.082.

[33] L. Wang, J.E. Martin, M. Felli, P.M. Carrica, Experiments and CFD for the propeller wake of a generic submarine operating near the surface, Ocean Eng. 206 (2020) 107304. https://doi.org/10.1016/j.oceaneng.2020.107304.
[34] Y.-H. Lin, X.-C. Li, The Investigation of a Sliding Mesh Model for Hydrodynamic Analysis of a SUBOFF Model in Turbulent Flow Fields, J. Mar. Sci. Eng. 8 (2020) 744. https://doi.org/10.3390/jmse8100744.
[35] J. Zou, G. Tan, H. Sun, J. Xu, Y. Hou, Numerical simulation of the ducted propeller and application to a semi-submerged vehicle, Pol. Marit. Res. nr 2 (2020). https://doi.org/10.2478/pomr-2020-0023.
[36] R.J. Paredes, M.T. Quintuña, M. Arias-Hidalgo, R. Datla, Numerical Flow Characterization around a Type 209 Submarine Using OpenFOAM, Fluids. 6 (2021) 66. https://doi.org/10.3390/fluids6020066.
[37] N.C. Groves, T.T. Huang, M.S. Chang, Geometric characteristics of DARPA SUBOFF models (DTRC Model Nos. 5470 and 5471), Naval Surface Warfare Center Carderock Division (NSWCCD), West Bethesda, MD, USA, 1989.
[38] T.T. Huang, H.L. Liu, N.C. Groves, Experiments of the DARPA SUBOFF Program, Naval Surface Warfare Center Carderock Division (NSWCCD), West Bethesda, MD, USA, 1989.
[39] T. Huang, H.L. Liu, Measurements of flows over an axisymmetric body with various appendages in a wind tunnel: the DARPA SUBOFF experimental program, in: Seoul, South Korea, 1994. https://trid.trb.org/view.aspx?id=449663.
[40] H.-L. Liu, T.T. Huang, Summary of DARPA Suboff Experimental Program Data, Naval Surface Warfare Center Carderock Division (NSWCCD), West Bethesda, MD, USA, 1998.
[41] D.C. Wilcox, Turbulence Modeling for CFD, 3rd edition, DCW Industries, La Cãnada, California, USA, 2006.
[42] D.C. Wilcox, Formulation of the k-w Turbulence Model Revisited, AIAA J. 46 (2008) 2823–2838. https://doi.org/10.2514/1.36541.
[43] ITTC, 7.5-03-02-03 Practical Guidelines for Ship CFD Applications, ITTC - Recomm. Proced. Guidel., 2014.
[44] Siemens, Star-CCM+ User Guide Version 15.02.007, (2020).
[45] F.R. Menter, Two-equation eddy-viscosity turbulence models for engineering applications, AIAA J. 32 (1994) 1598–1605. https://doi.org/10.2514/3.12149.
[46] S. Song, Y.K. Demirel, M. Atlar, An Investigation Into the Effect of Biofouling on Full-Scale Propeller Performance Using CFD, Proc. ASME 2019 38th Int. Conf. Ocean Offshore Arct. Eng. Vol. 2 CFD FSI, Glasgow, Scotland, UK, 2019.
[47] O.K. Kinaci, M.K. Gokce, A.D. Alkan, A. Kukner, On Self-propulsion Assessment of Marine Vehicles, Brodogr. Teor. Praksa Brodogr. Pomor. Teh. 69 (2018) 29–51. https://doi.org/10.21278/brod69403.
[48] P.M. Carrica, A.M. Castro, F. Stern, Self-propulsion computations using a speed controller and a discretized propeller with dynamic overset grids, J. Mar. Sci. Technol. 15 (2010) 316–330. https://doi.org/10.1007/s00773-010-0098-6.
[49] ITTC, 7.5-02-03-01.1 Testing and Extrapolation Methods, Propulsion, Performance Propulsion Test, ITTC - Recomm. Proced. Guidel., 2002.
[50] L.F. Richardson, The Approximate Arithmetical Solution by Finite Differences of Physical Problems Involving Differential Equations, with an Application to the Stresses in a Masonry Dam, Philos. Trans. R. Soc. Lond. Ser. Contain. Pap. Math. Phys. Character. 210 (1911) 307–357.
[51] P.J. Roache, Verification of Codes and Calculations, AIAA J. 36 (1998) 696–702. https://doi.org/10.2514/2.457.
[52] I.B. Celik, U. Ghia, P.J. Roache, C.J. Freitas, P.E. Raad, Procedure for Estimation and Reporting of Uncertainty Due to Discretization in CFD Applications, J. Fluids Eng. 130 (2008) 078001. https://doi.org/10.1115/1.2960953.

[53] ITTC, 7.5-03-01-01 Uncertainty Analysis in CFD, Verification and Validation Methodology and Procedures, ITTC - Recomm. Proced. Guidel., 1999.
[54] ITTC, 7.5-03-01-01 Uncertainty Analysis in CFD, Verification and Validation Methodology and Procedures, ITTC - Recomm. Proced. Guidel., 2014.
[55] R. Cosner, B. Oberkampf, C. Rumsey, C. Rahaim, T. Shih, AIAA Committee on Standards for Computational Fluid Dynamics: Status and Plans, 44th AIAA Aerosp. Sci. Meet. Exhib., American Institute of Aeronautics and Astronautics, Reno, Nevada, USA, 2006. https://doi.org/10.2514/6.2006-889.
[56] D. Uzun, S. Sezen, R. Ozyurt, M. Atlar, O. Turan, A CFD study: Influence of biofouling on a full-scale submarine, Appl. Ocean Res. 109 (2021) 102561. https://doi.org/10.1016/j.apor.2021.102561.
[57] F. Stern, R.V. Wilson, H.W. Coleman, E.G. Paterson, Comprehensive Approach to Verification and Validation of CFD Simulations—Part 1: Methodology and Procedures, J. Fluids Eng. 123 (2001) 793. https://doi.org/10.1115/1.1412235.
[58] J. Carlton, Marine Propellers and Propulsion, 4th edition, Butterworth-Heinemann, Amsterdam, 2018.
[59] Z.-Z. Wang, Y. Xiong, R. Wang, X.-R. Shen, C.-H. Zhong, Numerical study on scale effect of nominal wake of single screw ship, Ocean Eng. 104 (2015) 437–451. https://doi.org/10.1016/j.oceaneng.2015.05.029.
[60] ITTC, Report of Propulsion Committee, Wuxi, China, 2017.
[61] ITTC, 7.5-02-02-03 Resistance and Propulsion Test and Performance Prediction with Skin Frictional Drag Reduction, ITTC - Recomm. Proced. Guidel., 2017.
[62] ITTC, 7.5-02-03-01.1 Propulsion/Bollard Pull Test, ITTC - Recomm. Proced. Guidel., 2017.

Appendix A

Table A.1. *Self-propulsion characteristics at full-scale and 26 knots*

λ	n(rps)	K_T	$10K_Q$	$1-t$	J	$1-w$	η_0	η_H	η_R	η_D	P_D (kW)
1 (Full-scale CFD)	1.739	0.163	0.324	0.856	0.913	0.741	0.732	1.156	0.953	0.807	11003.655
2 (Extrapolated)	1.733	0.168	0.327	0.855	0.893	0.722	0.729	1.183	0.942	0.796	11157.157
24 (Extrapolated)	1.725	0.170	0.359	0.811	0.879	0.708	0.663	1.145	0.972	0.758	11715.179

Table A.2. *Self-propulsion characteristics at full-scale and 29 knots*

λ	n(rps)	K_T	$10K_Q$	$1-t$	J	$1-w$	η_0	η_H	η_R	η_D	P_D (kW)
1 (Full-scale CFD)	1.924	0.162	0.323	0.856	0.914	0.740	0.732	1.158	0.953	0.807	14878.373
2 (Extrapolated)	1.920	0.166	0.325	0.855	0.896	0.724	0.730	1.181	0.942	0.798	15061.825
24 (Extrapolated)	1.906	0.174	0.365	0.791	0.870	0.698	0.662	1.134	0.974	0.974	15998.845